Effect of free surfaces on the smectic-A–hexatic-B–crystal-E transitions in thin free-standing films of the liquid-crystal compound n-heptyl-4′-n-pentyloxybiphenyl-4-carboxylate (75OBC)

R. Geer,* T. Stoebe, and C. C. Huang
School of Physics and Astronomy, University of Minnesota, Minneapolis, Minnesota 55455
(Received 11 December 1992; revised manuscript received 8 March 1993)

An ac free-standing film calorimeter has been recently developed to investigate the physical properties of the smectic-A–hexatic-B–crystal-E transitions in free-standing films of the liquid-crystal compound n-heptyl-4′-n-pentyloxybiphenyl-4-carboxylate (75OBC). Due to the surface-enhanced order on free surfaces, we have discovered many new physical phenomena, e.g., a rich phase diagram, layer-by-layer transitions near a continuous transition, an interplay between a strong first-order surface transition and a nearby continuous transition, etc.

PACS number(s): 64.70.Md, 61.30.−v, 64.60.Kw

I. INTRODUCTION

Liquid-crystal free-standing films have provided one of the richest experimental systems in recent years. Multicriticality, two-dimensional melting, surface-induced phase transitions, layer-by-layer transitions, and dimensional crossover are examples of the wide range of phenomena which have been investigated in such free-standing films. This paper describes detailed heat-capacity data from free-standing films of the liquid-crystal compound n-heptyl-4′-n-pentyloxybiphenyl-4-carboxylate (75OBC). Section I reviews pertinent experimental and theoretical work with an emphasis on those systems studied in the context of surface induced order and two-dimensional melting. Section II deals with the experimental technique employed to measure the heat capacity as well as film thickness. Section III presents heat-capacity data as a function of thickness and temperature for 75OBC free-standing films. Electron- and x-ray diffraction data have been included for structural identification of the phases involved. Finally, the data are discussed and compared to the relevant theories concerning two-dimensional phase transitions and finite size effects.

A. Review of surface order in liquid-crystal films

The existence of enhanced positional and orientational order at free surfaces of thermotropic liquid crystals has been demonstrated by several experimental techniques on various compounds. Young *et al.* [1] demonstrated the feasibility of forming stable free-standing films of thermotropic liquid crystals over an opening roughly 1 cm in diameter. These uniform films are extremely well suited for the study of free-surface effects as well as any dimensional crossover exhibited by the phase transitions. Mechanical (torsional oscillator) measurements of thin, free-standing liquid-crystal films of N-(4-n-butyloxybenzylidene)-4-n-octylaniline (4O.8) showed anomalous features attributed to the freezing of the surface layers into the crystal-B (Cry-B) phase [2]. Surface and interior smectic-A (Sm-A)–Cry-B transitions are separated by about 8 K. Similar results suggesting surface crystal order were obtained from mechanical measurements of n-hexyl-4′-n-pentyloxy-biphenyl-4-carboxylate (65OBC) [3]. (Since hexatic phases do not respond to a shear, this technique is insensitive to surface hexatic order.) X-ray measurements of 65OBC report a sudden stabilization of bond-orientational order below the Sm-A–hexatic-B (Hex-B) transition temperature [4]. This was also attributed to a surface crystalline phase and is consistent with the oscillator measurements. Recently, electron-diffraction studies have tentatively identified this as a surface Cry-E phase [5].

Tilted smectic phases have also demonstrated surface order. In a beautiful series of ellipsometry experiments Heinekamp *et al.* [6] measured the tilt angle of the smectic-C (Sm-C) phase as a function of temperature for p-(n-decyloxybenzylidene)-p-amino-(2-methylbutyl)-cinnamate (DOBAMBC) free-standing films varying from two to ten molecular layers in thickness. They described their data in a mean-field coupled-plane model which implied separate surface and interior behavior. Amador and Pershan [7] repeated these measurements in conjunction with dynamic light-scattering experiments to study the surface Sm-C transition in terms of two-dimensional melting theory. Upon close examination, the surface tilt was found to possess a discontinuous slope which is consistent with the universal jump in the superfluid density as described by Nelson and Kosterlitz [8].

X-ray measurements by Sirota *et al.* [9] revealed surface smectic-I (Sm-I) order in thin films of N-(4′-n-heptyloxybenzylidene)-4-n-heptylanilne (7O.7). The surface-SmI–interior-Sm-C phase was characterized by a combination of a broad, diffuse scattering profile indicative of the shorter in-plane correlation lengths of the Sm-C phase and a sharper peak due to the more correlated Sm-I surface order. The most unique feature of this work is that hexatic phases do not appear in bulk samples of this material, but instead exist only as surface stabilized phases in free-standing films. Amador *et al.* [10] performed synchrotron x-ray measurements near the surface

1063-651X/93/48(1)/408(20)/$06.00

and interior Sm-I transitions reported by Sirota *et al.* [9]. This work measured the in-plane positional correlation lengths as determined from fitting to the in-plane diffraction peaks. At the surface transition a discontinuous jump was observed in this correlation length suggesting a discontinuous surface Sm-C–Sm-I transition. No such discontinuity was seen for the interior Sm-C–Sm-I transition.

Surface order in liquid-crystal free-standing films appears in many phases for many different compounds. Yet it is interesting to note that no surface order was seen in racemic 4''-(2'-methylbutyl)phenyl-4'-*n*-octyloxybiphenyl-4-carboxylate (2M4P8OBC or 8OSI) in the x-ray studies by Brock *et al.* [11]. The weak χ structure in the thick-film Sm-C phase developed continuously as shown quite nicely by the order-parameter profiles. No scattering attributed to surface order was seen in the thin (four-layer) films either. Our preliminary calorimetric studies on four- and five-layer films of 8OSI clearly exhibit separate surface and interior transitions. Detailed heat-capacity studies on the free-standing films of this compound will be conducted in the near future.

Some of the most recent investigations of surface induced order in free-standing liquid-crystal films concerns another set of x-ray experiments on 7O.7 by Tweet *et al.* [12] and on 8CB by Gierlotka, Lambouy, and de Jeu [13]. In the region where Sirota *et al.* [9] reported a surface-Sm-I–interior-Sm-C phase, small-angle x-ray diffraction (specular reflectivity) was used to discern the tilt and spatial fluctuation profiles of the film. In work very analogous to that of Pomerantz and Segmuller [14] on Langmuir-Blodgett films, Tweet *et al.* [12] employed an analogy with N-slit diffraction to fit their data. By convoluting an assumed structure factor for the film with a Gaussian distribution for the molecular center-of-mass fluctuations parallel to the layer normal, they were able to determine the layer-fluctuation profile for the film.

B. Review of surface critical phenomena

The appearance of surface order for various liquid-crystal compounds has provided experimental systems for which to apply theories of surface critical phenomena. Surface transitions have been treated in phenomenological mean-field theories and yield very insightful results. As in Ref. [15], we can define bulk and surface free energies for a scalar order parameter $m(\mathbf{r})$, where $\mathbf{r}=(z,\rho)$ in a cylindrical coordinate system (appropriate for free-standing films),

$$F_b/T=\int d\rho\int_0^L dz\{\tfrac{1}{2}Am^2(\mathbf{r})+\tfrac{1}{4}Bm^4(\mathbf{r}) -H(\mathbf{r})m(\mathbf{r})+\tfrac{1}{2}C[\nabla_{\mathbf{r}}m(\mathbf{r})]^2\}\ , \tag{1a}$$

$$F_s/T=\int d\rho\{\tfrac{1}{2}C\lambda^{-1}[m^2(\rho,z=0)+m^2(\rho,z=L)] -H_1(\rho)[m(\rho,z=0)+m(\rho,z=L)]\}\ . \tag{1b}$$

A, B, and C are the usual mean-field coefficients. H is an external magnetic field and H_1 is a suitably defined surface field. The coefficient $C\lambda^{-1}$ determines the energy scale for the surface free energy (F_s), where λ has units of length. By integrating over ρ in Eq. (1), the bulk free energy (F_b) is reduced to an integration over the thickness, L, of the sample, and the surface free energy depends only on the average magnetization at the surfaces. Functionally minimizing with respect to $m(z)$ leads to equations for the order parameter as a function of z. The surface energy terms furnish boundary conditions

$$Am(z)+Bm^3(z)-C\left[\frac{\partial^2 m}{\partial z^2}\right]=H\ , \tag{2}$$

$$\frac{\partial m}{\partial z}-\frac{m}{\lambda}=-\frac{1}{C}H_1,\quad z=0\ , \tag{3a}$$

$$\frac{\partial m}{\partial z}+\frac{m}{\lambda}=\frac{1}{C}H_1,\quad z=L\ . \tag{3b}$$

Letting L become infinite and ignoring spatial variations in m, the standard mean-field results are obtained for the temperature dependence of m (denoted m_b for $L=\infty$), $\xi_b^{\pm}$ and $\chi_b^{\pm}$. For films of finite thickness it is possible to calculate the order parameter profiles. Following Ref. [15], the definition $\eta=z/\xi_b^+$ has been adopted. For zero bulk field H and small, finite H_1, Eq. (2) can be integrated (invoking boundary conditions) to yield the order parameter profile as a function of the scaled variable η,

$$m(\eta)=m_b-(m_b-m_1)\times\cosh[\eta-L/(2\xi_b^+)]/\cosh[L/(2\xi_b^+)]\ , \tag{4a}$$

where

$$m_1=\{(\lambda/\xi_b^+)m_b\tanh[L/2\xi_b^+] +H_1\lambda/C\}/\{1+(\lambda/\xi_b^+)\tanh[L/2\xi_b^+]\}\ . \tag{4b}$$

Since $m(0)=m_1$, it is akin to a surface order. Thus dm_1/dH_1 is proportional to a surface susceptibility

$$\frac{dm_1}{dH_1}=\frac{\lambda/C}{1+(\lambda/\xi_b^+)\tanh[L/2\xi_b^+]}\ . \tag{5}$$

Notice that Eq. (5) diverges for $1=-(\lambda/\xi_b^+)\tanh[L/2\xi_b^+]$. This occurs for a negative surface energy, such as that implied by the ordering at liquid-crystal free surfaces, and denotes a separate surface phase transition. Although this transition occurs at the surface, in a two-dimensional (2D) geometry, it is due to enhanced correlations from a nearby bulk transition [this is implicit in the rescaling of z in Eq. (2)]. This theory makes no predictions for 2D ordering at surfaces, such as that implied in the work by Amador and Pershan [7]. It serves to illustrate surface properties of finite thickness films. Equation (5) then predicts a surface transition at T_s determined by the equation

$$\lambda^{-1}=-[\xi_b^+(T_s)]^{-1}\tanh[L/2\xi_b^+(T_s)]\ . \tag{6}$$

A variation of this equation was used in Ref. [6] to de-

scribe the dependence of transition temperatures on thickness in Sm-A–Sm-C transitions. The application of this theory to 75OBC is discussed below.

To investigate the effects of enhanced surface order on normal finite-size phenomena, Li *et al.* [16], motivated by the heat-capacity measurements presented here, examined the heat capacity of layered films in terms of a simple Ising model. Results were obtained from an exact solution of the problem, and compared with those from finite-size-corrected mean-field theory. Theoretically, the Sm-A–Hex-B transition in liquid-crystal free-standing films can be represented as coupled planes of 2D XY spins. This problem cannot be solved analytically, and there is, as yet, no consensus on computer simulation studies of this system. Rather, Li *et al.* [16] modeled an N-layer film as N coupled 1D Ising chains. This essentially collapses each 2D smectic layer onto an infinite line of Ising spins. For this 2D "strip" of Ising spins there is no true singularity in the heat capacity, although there is a well-defined maximum. For purposes of comparison with experimental data, these maxima define the transition temperatures.

The model Hamiltonian for an N-layer anisotropic system is

$$H=\sum_{\alpha=1}^{N}\sum_{\langle i,j\rangle}J_H^{\alpha}\sigma_i^{\alpha}\sigma_j^{\alpha}+\sum_{\alpha=1}^{N-1}\sum_{i}J_V^{\alpha}\sigma_i^{\alpha}\sigma_i^{\alpha+1}\,, \tag{7}$$

where the σ_i are Ising spins and the $J_{H(V)}$ are intra-(inter-) layer coupling constants and α is the layer index. To include the effects of the free surfaces, the value of the intralayer coupling of the surface layers is changed, giving

$$H=\sum_{i}J_s(\sigma_i^1\sigma_{i+1}^1+\sigma_i^N\sigma_{i+1}^N)+\sum_{\alpha=2}^{N-1}\sum_{i}J_H\sigma_i^{\alpha}\sigma_{i+1}^{\alpha}+\sum_{\alpha=2}^{N-1}\sum_{i}J_v\sigma_i^{\alpha}\sigma_i^{\alpha+1}\,, \tag{8}$$

where J_S is an enhanced surface coupling. It was found that the difference between transition temperatures for infinite and finite-thickness films could be expressed in terms of a scaling function when the film thickness was scaled by a characteristic length ξ_s. Bulk behavior is not expected unless $N\gg\xi_s$, and a "surface-dominated" regime only exists for films significantly thinner than ξ_s. Predictions of this theory are compared with heat capacity data of 75OBC below.

C. Brief review of two-dimensional melting

As the thickness of the film is reduced, it becomes necessary to consider the explicit nature of the liquid-hexatic transition in two dimensions. This statement is somewhat redundant since the theory of 2D melting in solids given by Halperin and Nelson [17] first predicted the hexatic phase. Their work extended that of Kosterlitz and Thouless [18], which described the defect-mediated continuous transition for a two-component order parameter (e.g., the planar spin model, superfluidity, etc.) in 2D. Phases were differentiated by the long-range behavior of the order-parameter correlation function: decaying exponentially with separation in the disordered phase and algebraically in the ordered phase. The transitions were driven by the appearance of topological defects as the temperature was increased. In the melting of solids, Halperin and Nelson [17] suggested the possibility of a pair of such transitions. At low temperatures, algebraically decaying positional order would give way to an orientationally ordered phase (christened hexatic for systems with sixfold symmetry). This intermediate phase, in turn, melts into a liquid phase at a higher temperature.

The liquid-hexatic transition is isomorphic to the Kosterlitz-Thouless (KT) transition [18] for the planar-spin model wherein the topological defects are spin vortices. Detailed heat-capacity calculations have been made for such a model by Berker and Nelson [19] and Solla and Riedel [20]. Using the KT recursion relations, the free energy was calculated as vortex pairs become screened from one another and unbind, initiating the transition. Due to the form of the recursion relations, and the temperature dependence of the correlation function, all derivatives of the vortex free energy vanish at the transition temperature, yielding no singularity in the heat capacity C_v. Low-temperature expansions predict an exponential rise in C_v as vortex pairs are excited. Following the unbinding at high temperatures, a dilute vortex gas is formed. This results in an additional contribution to the heat capacity that is only weakly temperature dependent. Between these limits, calculations of the vortex free energy show a broad heat-capacity maximum located at approximately $1.3T_c$. This maximum is attributed to the rapid dissociation of tightly bound pairs. Solla and Riedel's results [20] for heat capacity are shown in Fig. 1. Because no heat-capacity feature arises from the divergence of the correlation length, the shape of C_V in

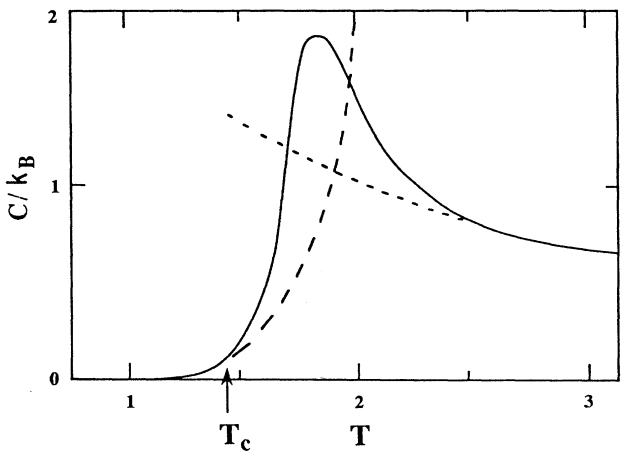

FIG. 1. Temperature dependence of the heat capacity (in the unit of the Boltzmann constant k_B) of the 2D planar spin model [20]. The solid curve is generated by a renormalization-group calculation of the free energy. The results from a low- (high-) temperature approximation are shown as a long- (short-) dashed line. The arrow indicates the transition temperature (T_c) where vortex pairs begin to unbind. There is no singular behavior in the heat capacity at T_c. The broad maximum above T_c is due to rapid dissociation of vortex pairs as screening from free vortices increases.

Fig. 1 is nonuniversal and depends on several system parameters. This is an interesting exception to the ideas of universality commonly held for continuous order-disorder phase transitions. It is not surprising, however, in light of the manner in which the correlation length diverges at the transition. The nonuniversality clearly complicates any comparison of experimental data to Fig. 1 and perhaps the most significant feature is the excess heat capacity above the transition.

Certain Monte Carlo simulations [21] and quantum path-integral calculations [22] have reproduced the results of Ref. [20]. Other Monte Carlo work has shown a sharp and symmetric cusplike maximum much closer to the transition temperature [23]. Finite-size effects and long equlibration times are often cited as reasons for the discrepancies among different simulations [24]. At least two different experiments [25] have been conducted to explore the nature of this unique feature of the heat capacity near the KT transition temperature. So far the experimental results are not conclusive.

II. EXPERIMENTAL METHODS

A. Calorimeter setup

The oven used for our studies provides a controlled environment for the creation of free-standing films and the measurement of the heat capacity of the film using ac calorimetry (Fig. 2) [26]. The oven consists of two cylindrical stages, one enclosing the other. The inner stage is covered with windings of resistive wire for regulation of the film's average temperature. The oven is filled with 99.9995% pure argon exchange gas at 0.5 atm. Chopped infrared laser light ($\omega/2\pi=35$ Hz, $\lambda_{\text{laser}}=3.4$ μm) is incident on the film, resulting in an absorbed power q_{abs}, which induces a periodic temperature oscillation ΔT_{ac}. This is related to the film heat capacity. To allow for observation, infrared radiation heating, and thickness measurements of the films, *I*2-ir fused-quartz windows with large transmission coefficients at 3.4 μm are located in the top plates of both stages. Inside the inner stage, free-standing films are spread over a circular opening (9 mm diameter) in a stainless-steel plate. Films are spread by the movement of a glass cover slip across the opening in the film plate.

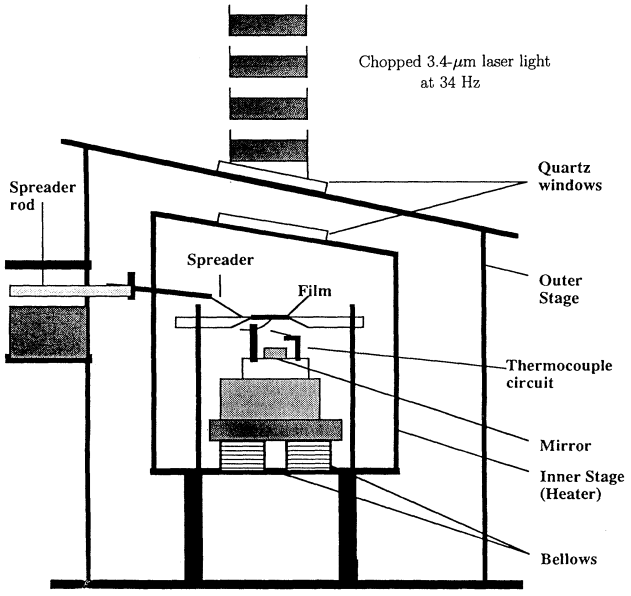

FIG. 2. Free-standing film calorimeter schematic.

So far we have been able to prepare uniform free-standing films from five different *nm*OBC compounds, namely, 3(10)OBC, 37OBC, 46OBC, 65OBC, and 75OBC. One general guideline obtained from our experience is that those compounds with overly short alkyl chains are not good candidates for preparing uniform free-standing films. Furthermore, at least 2000 films have been prepared in our laboratory and we have never observed a stable one-layer film. The thinnest film reported in our research work is therefore two layers thick. Although there may be differences in the physical properties of the one- and two-layer films, this experimental limitation prevents us from addressing this question.

The film-temperature sensing circuit consists of a pair of constantan-chromel thermocouples mounted one above the other parallel to the laser beam. The upper thermocouple, located only 25 μm below the film, senses a temperature oscillation amplitude due to the film and the surrounding exchange gas as well as that due to direct heating by transmitted laser radiation (for thin films laser transmittance is often greater than 98%). The lower thermocouple is mounted approximately 5 mm below the upper. Since the thermal diffusion length for argon gas at $f=35$ Hz and $P=\frac{1}{2}$ atm is approximately 0.7 mm, the lower thermocouple is quite insensitive to temperature variations of the film. The two thermocouples are connected in series, with the lower one reversed, giving a difference of thermal voltages and thus subtracting the laser contribution from the film signal. This way, ΔT_{ac} is measured directly. This subtraction is crucial since direct heating by the laser can be as much as 50 times larger than the change in film signal at a phase transition. In some circumstances, the lower thermocouple can also be used independently to monitor laser power intensity through the transition. A detailed account of our calorimeter was published in Ref. [26].

Two important informations relevant to this paper are the following. First, to demonstrate that the ac operating frequency $f=35$ Hz is appropriate, a typical frequency response curve [namely, $\log_{10}(f\Delta T_{\text{ac}})$ vs the logarithm of f] is shown in Fig. 3. The data were obtained from a 65OBC 50-layer film and exhibited a flat regime between 16 and 80 Hz. Second, in most of the experimental runs, we chose ΔT_{ac} to be about 5–10 mK and the ramping rates of the sample temperature were generally 10–20 mK/min. In certain instances the scanning rates as low as 0.5 mK/min were used near the transition temperature.

We have ensured that our measured signal is related to the heat capacity of the liquid-crystal films by successfully completing the following four experiments: (1) Em-

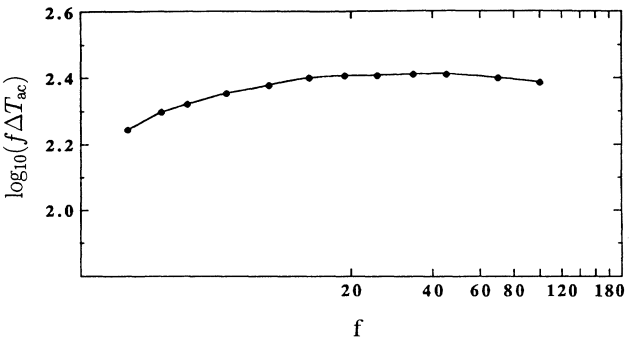

FIG. 3. Frequency response curve [$\log_{10}(f\Delta T_{ac})$ vs f] obtained from a 65OBC 50-layer film. The solid line is a guide for the eye.

ploying detectors much more sensitive to 3.4-μm radiation (namely PbSe detectors), we simultaneously measured the transmittance and reflectance of a 100-layer film of 46OBC. The results showed that the amount of radiation absorbed by the films was independent of temperature throughout a region including the Sm-A–Hex-B transition. (2) In the case of thick films (>400 layers), no signal can be detected by the lower thermocouple junction (no laser radiation is transmitted through the film), while the upper thermocouple yields a signal related to the heat capacity [27], which is in very good agreement with the results from our bulk calorimeter. (3) In the case of thin films, the transmitted laser radiation detected by the lower thermocouple junction shows no change through the Sm-A–Hex-B transition. (4) Away from the transition region, the measured heat capacity is proportional to the film thickness (see Fig. 4 and discussions in Sec. II B). These results strongly suggest that our measured signal is related to the heat capacity of the liquid-crystal films (and is not due to any other effect, such as critical opalescence or change in absorption, etc.).

B. Determination of film thickness

Since most thermotropic liquid crystal molecules range from 25 to 35 Å in length, free-standing film thicknesses vary between 50 Å and fractions of micrometers. For a large region of thickness, visible light provides a probe to determine the number of layers present. For very thin films (less than 12 layers) the layer number can be determined by the reflected intensity of low-power laser light [28]. The following equations give the reflectance of polarized light for a uniaxial dielectric slab:

$$R_{\parallel}=(n_{\parallel}^2\cos^2 i-\cos^2 r_{\parallel})^2\sin^2 a_{\parallel} \times[4n_{\parallel}^2\cos^2 i\cos^2 r_{\parallel}+(n_{\parallel}^2\cos^2 i-\cos^2 r_{\parallel})^2\sin^2 a_{\parallel}]^{-1}, \quad (9)$$

$$R_{\perp}=(\cos^2 i-n_{\perp}^2\cos^2 r_{\perp})^2\sin^2 a_{\perp} \times[4n_{\perp}^2\cos^2 i\cos^2 r_{\perp}+(\cos^2 i-n_{\perp}^2\cos^2 r_{\perp})^2\sin^2 a_{\perp}]^{-1},$$

where i is the angle of incidence, $r_{\parallel}$ ($r_{\perp}$) is the angle of refraction for the components parallel (perpendicular) to the plane of incidence, $n_{\parallel}$ ($n_{\perp}$) is the index of refraction for parallel (perpendicular) components, $a_{\parallel}=n_{\parallel}kh\cos(r_{\parallel})$, $a_{\perp}=n_{\perp}kh\cos(r_{\perp})$, k is the wave vector of light, and h is the slab thickness. For small values of h the reflected intensity has a quadratic thickness dependence. Since h represents a discrete number of layers, the thickness may be calibrated by creating many films and observing the various quantized intensities. This works very well for $N<12$. Above this range the reflected intensity no longer scales with the square of the thickness. For thicker films, the constructive interference of incident white light can be used to determine layer number [29]. The thinnest films ($2<N<10$) range from nearly black to dark gray in color from the destructive interference of the incident light. For $10<N<25$, reflected light increases and color ranges from whitish to pale yellow. Thicker films develop the following color spectrum: $N=30$ (orange), $N=50$ (red), $N=60$ (blue), $N=70$ (green), $N=85$ (yellow), $N=120$ (red), and so on. The colors of the second- and third-order cycles are paler and can be differentiated from colors of the first cycle. For films greater than 300 layers in thickness, the color oscillates between pale shades of pink and green. For $N>50$, this method works well (to within 5–10%) simply by visual observation of the film.

For thinner films ($12<N<50$), visual inspection was not entirely adequate for determining film thickness due to a lack of contrast in the color spectrum. For certain features seen in the heat capacity of 75OBC it was important to more accurately measure layer number in this region. It was necessary to deduce the thickness from the measured temperature oscillation (ΔT_{ac}) of films in the Sm-A phase. This also allowed for the calibration of the film heat capacity in absolute units. From Ref. [30] the apparent heat capacity per unit area C^*/A is given by

$$(C^*/A)^2=(C_f/A)^2+2\delta^*C_f/A+2\delta^{*2}, \quad (10)$$

where $(C^*/A)=q_{abs}/2\omega\Delta T_{ac}$, C_f/A is the heat capacity per unit area of the film, and δ^* is the effective contribution of the argon exchange gas and the thermocouple. Assuming $C_f/A=c_L\epsilon N$, where ϵ is the layer spacing, c_L is the specific heat for bulk nmOBC liquid crystal, and A is the cross-sectional probing area of the film, the temperature oscillation amplitude of the film can be expressed as

$$\Delta T_{ac}=\frac{q_{inc}(1-e^{-N/\lambda})}{2\sqrt{2}\omega\delta^*\left[1+\frac{c_L\epsilon N}{\delta^*}+\frac{(c_L\epsilon N)^2}{2\delta^*}\right]^{1/2}}. \quad (11)$$

q_{inc} is the incident laser power per unit area and λ_{opt} is the absorption length for 3.4-μm radiation in a smectic film (in units of layer spacing). From estimates of thermocouple and gas contributions to the measured heat capacity,

$$\delta^*=3.81\times10^{-5}\ \mathrm{J/cm^2\,K}.$$

Using typical values for the heat capacity of the relevant nmOBC compounds in the Sm-A phase, the ratio $c_L\epsilon/\delta^*=0.018$. To test this assumption and provide a method of determining film thickness for $12<N<60$, Eq.

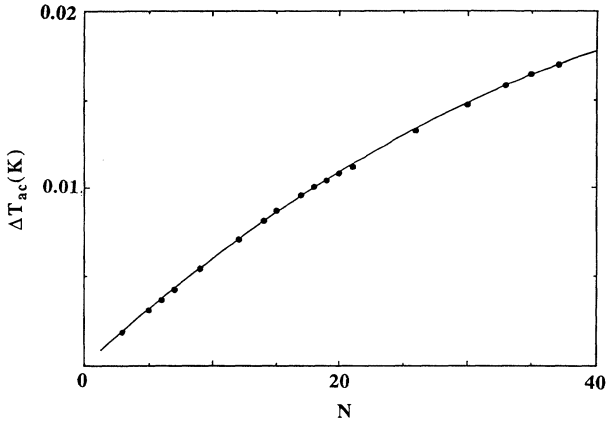

FIG. 4. Temperature oscillation amplitude ΔT_{ac} as a function of layer number. The solid dots are measured thicknesses determined from intensity of reflected 0.63-μm laser light. The line is calculated from Eq. (11) for the liquid-crystal absorption length $\lambda_{opt}=250$ lasers.

(11) was fitted to temperature oscillation amplitude versus layer number for thin films of 75OBC. The thicknesses of these films were obtained from 0.63-μm laser-light reflectance as described earlier. Although quadratic dependence of intensity on N no longer holds for $N>12$, it is possible to determine film thickness by spreading many films until the measured intensities begin to repeat due to the quantized nature of the layer structure. Also, requiring that the derivative of the intensity as a function of thickness be a smooth, monotonically decreasing function of N (until the first reflectance maximum is reached) provides a second check on layer number. Combining these two techniques, films ranging from 2 to 35 layers in thickness were spread. Assuming $\lambda_{opt}=250$ (roughly determined from absorption of thick *nm*OBC films), Eq. (11) was fitted to these data yielding values for the incident power and a check on the specific heat of the film:

$$q_{inc}=7.6\times10^{-4}\ \mathrm{W/cm^2}\ ,$$

$$c_L\epsilon/\delta^*=0.017\pm0.001\ .$$

Figure 4 shows the ΔT_{ac} versus the layer number (N) along with the fitted curve for $N<40$. Within the error values for the fitted parameters, the fitted curve is somewhat insensitive to the value of λ_{opt} ranging from 200 to 300 layers. Note: to demonstrate the simple relation between ΔT_{ac} and N in Fig. 4, we used all the laser power without attenuation. During the course of our heat capacity measurements, the laser radiation is attenuated for film thickness greater than about 20 layers. In other words, we always keep the magnitude of ΔT_{ac} below approximately 10 mK.

III. HEAT-CAPACITY DATA FOR 75OBC FREE-STANDING FILMS

A. Identification of phases in 75OBC free-standing films

To characterize the free-standing film calorimeter as well as the samples used, heat capacities for thick films of 65OBC were measured (Fig. 5) to compare with results from bulk samples [30]. These data were fitted to the power-law expression used by Pitchford *et al.* [31] to describe the Sm-A–Hex-B transition in bulk *nm*OBC (*n*-alkyl-4′-*n*-alkoxybiphenyl-4-carboxylate) samples. The agreement in the heat capacity exponent $\alpha=0.59\pm0.03$ is very good. Even though the fitted amplitude ratio $A^+/A^-=0.99\pm0.08$ is slightly larger than the value for the bulk sample ($A^+/A^-=0.85\pm0.08$), they are still within our fitting statistical errors. Here A^+ (A^-) represents the amplitude of the singular term in describing the heat-capacity anomaly above (below) T_c [32]. The thick-film heat-capacity anomaly was actually sharper than that of bulk samples and could be fitted by a power law closer to the transition temperature (8 mK). This is probably due to the single smectic domain present in free-standing films as opposed to the polydomain character of bulk samples.

As film thickness decreases, effects due to the free surfaces become apparent. Figure 6 shows heat capacity scans (cooling) for eight- and ten-layer 75OBC films. The large peak associated with the bulk (interior) transition is still evident; however, two higher temperature anomalies are discernible. The highest temperature peak (~71 °C) corresponds to a liquid-hexatic transition of the top and bottom surface layers. The second peak results from a liquid-hexatic transition of *the layers adjacent to the surface.* The layer-by-layer nature of the liquid-hexatic transition is reminiscent of wetting phenomena in other systems. Immediately below the interior liquid-hexatic transitions of both the ten- and eight-layer data, abrupt heat-capacity jumps can be seen. These are due to a surface hexatic–Cry-E phase transition which will be discussed in detail below.

To determine the phases associated with the extra liquid-hexatic peaks and the abrupt jumps in the thin film heat capacity data, electron-beam and x-ray diffraction studies were undertaken. The electron diffraction was performed at the Roswell Park Cancer Institute in collaboration with M. Cheng and J. T. Ho of the State University of New York at Buffalo. X-ray investigations were undertaken at AT&T Bell Laboratories and Brookhaven National Laboratory in conjunction with R. Pindak.

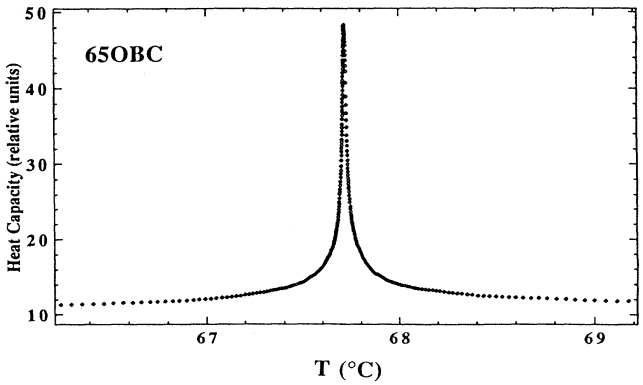

FIG. 5. Heat capacity of a thick 65OBC film (> 300 layers) in the vicinity of the Sm-A–Hex-B transition.

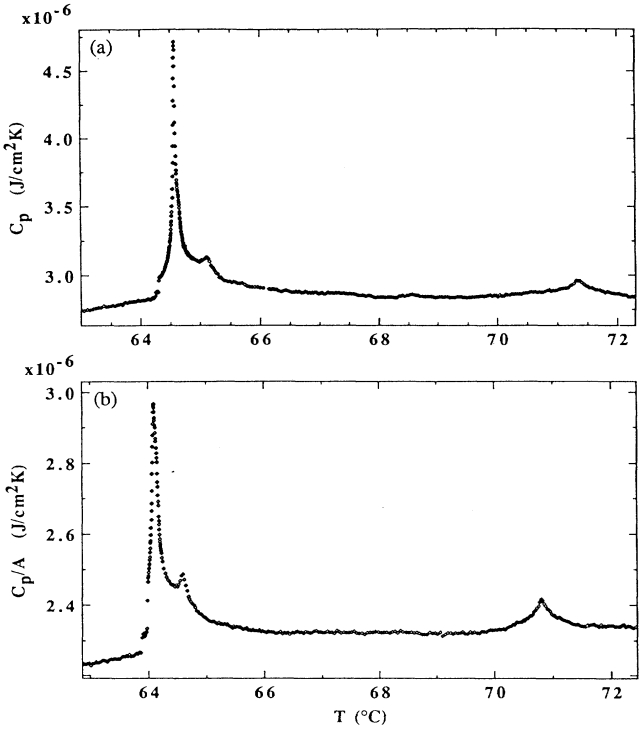

FIG. 6. Heat-capacity data from (a) ten- and (b) eight-layer 75OBC films. The AB_s transitions are apparent near 71 °C. The two lower-temperature peaks correspond to hexatic ordering in the AB_{AS} and AB_i transitions. The heat-capacity jumps near (a) 64.5 °C and (b) 64 °C signal the surface Hex-B–Cry-E transition.

Figure 7 displays a χ scan for a three-layer 75OBC film 2.06 °C above the surface hexatic-Cry-E transition. (Due to the sudden appearance of the Cry-E order and its unmistakable diffraction signature it was used to calibrate the temperature scales between the heat-capacity and electron-diffraction measurements.) This is a scan in reciprocal space about the axis normal to the layers. For a normal fluid phase such a scan would yield a constant scattered intensity. The sixfold modulation seen in the data, however, positively identifies hexatic order in the film. This modulation results from local positional order induced by hexatic (bond-orientational) order. The data were taken at a temperature between the two heat-capacity peaks in Fig. 8(b). Above 71 °C [the position of the high-temperature peaks in Figs. 8(a) and 8(b)] no such modulation can be resolved in the diffraction data. The diffraction data, therefore, imply that the high-temperature peak is due to a surface liquid-hexatic transition (since free-standing films acquire order from the surface inwards) while the second peak corresponds to hexatic order developing in the layers adjacent to the surface (this will become more apparent from the four- and five-layer heat capacity data). In the remainder of this paper the liquid-hexatic transition of the outermost surface layers will be referred to as the surface Sm-A–Hex-B (abbreviated AB_s) transition. The liquid-hexatic transition

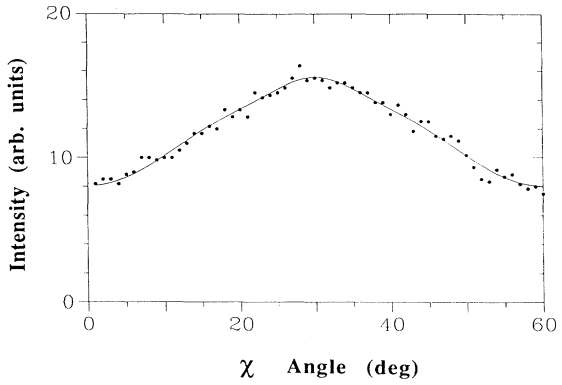

FIG. 7. Diffracted electron intensity from a three-layer 75OBC film. The data were taken 2.06 K above the surface hexatic–Cry-E transition. This temperature is between the surface-layer and interior-layer transitions. The angle χ refers to a rotation in reciprocal space about the layer normal. The solid line is a fit similar to that described in Ref. [37].

of the layers adjacent to the surface layers will be referred to as the adjacent-to-surface Sm-A–Hex-B (abbreviated AB_{AS}) transition. Many of the interior peaks for films greater than eight layers exhibit a high-temperature shoulder which could be associated with a third liquid-hexatic transition. For the remainder of this paper the development of additional hexatic ordering at a tempera-

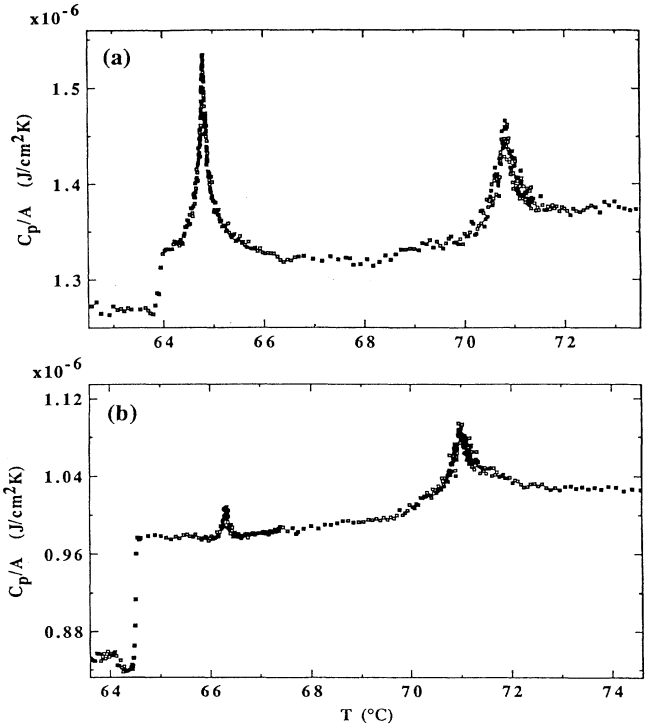

FIG. 8. Heat-capacity data from (a) four-layer and (b) three-layer 75OBC films. The existence of a single interior transition for both films confirms the identification of the high-temperature peak as an AB_s transition.

ture below the AB_s and AB_{AS} transitions will simply be characterized by the major heat-capacity peak ($N > 5$) and referred to as *interior* Sm-A–Hex-B (abbreviated AB_i) transitions.

Similar diffraction studies were performed to identify the phase associated with the abrupt jump below the liquid-hexatic transitions. Figure 9 shows an electron-beam diffraction pattern from a 75OBC five-layer film at 64.2°C (below the heat-capacity jumps). It beautifully illustrates the ordering present in the film. Two sets of ten spots can be seen with a sixfold symmetric set of diffuse arcs (the χ scan of Fig. 7 is a 60° angular scan along one of these arcs for a three-layer film). The sharp spots are characteristic of quasi-long-range crystalline and herringbone order indicative of the Cry-E phase while the diffuse arcs confirm that a portion of the film is still hexatic. The sharp heat-capacity jumps are thus associated with a hexatic–Cry-E transition of some region of the film.

X-ray investigations of this crystal phase were undertaken to determine the extent to which the above Cry-E order was correlated between layers. Figure 10 shows **q** (momentum transfer) scans along the **c*** direction through the (1,1,0) peak (see inset) for a four- and five-layer film at 59 °C and 60.2 °C, respectively. The four-layer data obtained at a lower temperature clearly show the interlayer correlations present for a completely crystalline film. The five-layer data lack such structure, showing a broad scattering peak due to the molecular form factor. The **q** scans along the (1,1,0) direction for both film thicknesses are shown in Fig. 11. Both scans were taken at temperatures well above the interior Hex-B–Cry-E transition and the lattice constants were indexed for local hexagonal order in the Hex-B phase. The peak positions [$q = 0.9735(2\pi/a_B)$] and widths (3.6×10^{-3} Å^{-1}) in Fig. 11 are indicative of long-range herringbone packing order in the Cry-E phase. Thus, for temperatures between the lower-temperature Hex-B–Cry-E transition (about 59 °C) and the abrupt drops seen immediately below the interior Sm-A–Hex-B transition, in-plane scans reveal crystalline order, yet no interlayer correlations were observed. We conclude that this phase is characterized by uncorrelated Cry-E surfaces separated by a hexatic interior. This conclusion is not unexpected since surface hexatic order also appears well above the interior hexatic transitions. It should be noted that previous x-ray [4] and torsional oscillator [3] measurements on free-standing liquid-crystal films also implied a surface crystal phase in 65OBC (recent heat-capacity investigations place this surface crystal transition at 65.2 °C).

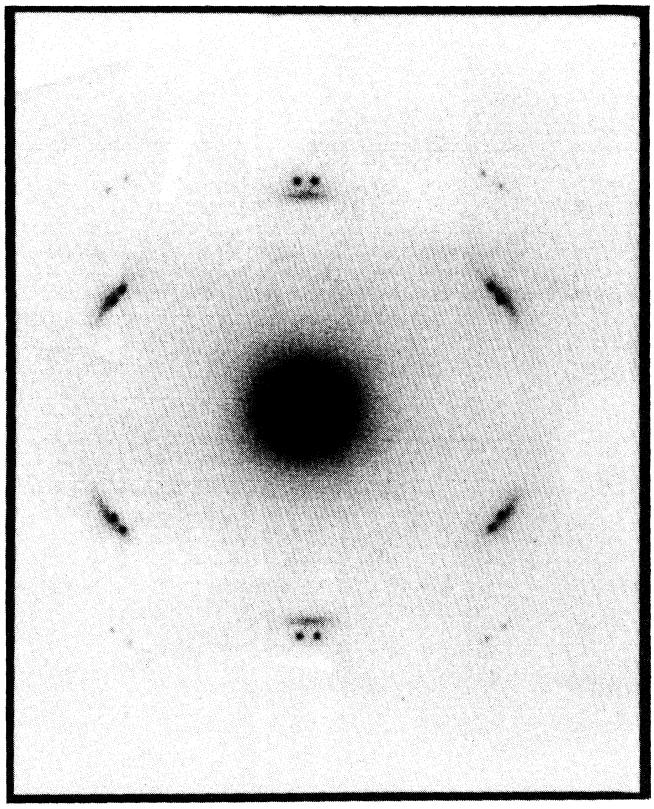

FIG. 9. Electron-diffraction pattern from a five-layer 75OBC film. The sixfold symmetric diffuse scattering identifies interior hexatic order, while two sets of Cry-E spots reflect separate Cry-E surface domains.

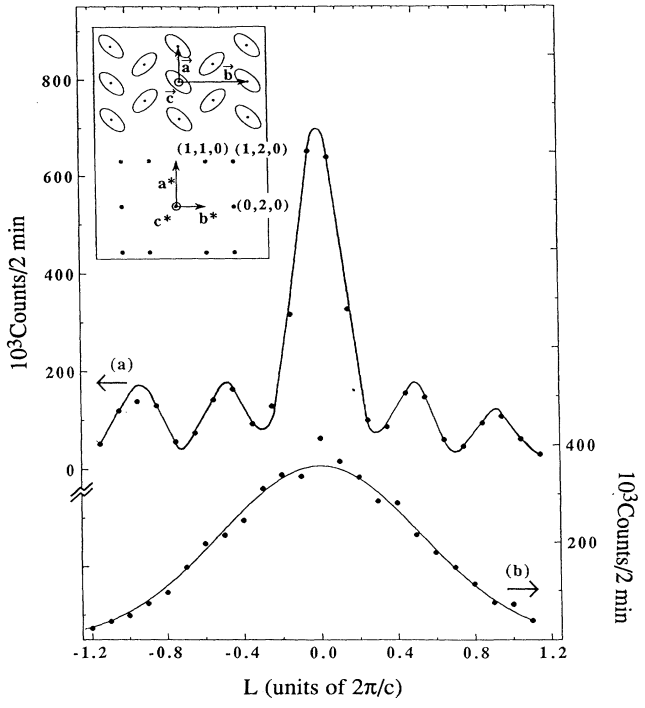

FIG. 10. X-ray scattering profiles obtained from **q** (momentum transfer) scans along c^* direction through the (1,1,0) peak (see inset) for (a) four- and (b) five-layer films at 59 °C and 60.2 °C, respectively. The inset describes the real-space and reciprocal-space lattice vectors for the Cry-E order. The modulation of the four-layer data which is taken at a low temperature shows interlayer correlations indicative of a crystal phase. This is not the case for (b).

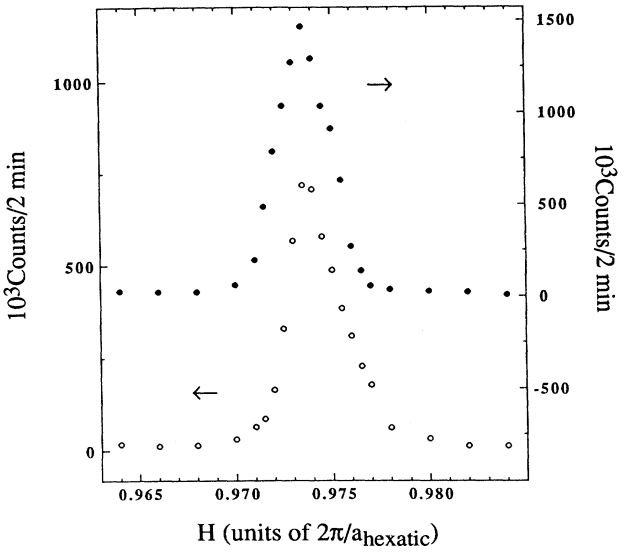

FIG. 11. X-ray scattering profiles (open circles, four-layer film; solid dots, five-layer film) obtained from **q** scans along the (1,1,0) peaks of the same films as reported in Fig. 10. Both exhibit Cry-*E* ordering in the films. Along with the results in Fig. 10, this demonstrates that the Cry-*E* order present in both films is correlated between the layers for the four-layer film but not in the five-layer film. This implies the existence of surface Cry-*E* order for temperature greater than 59 °C.

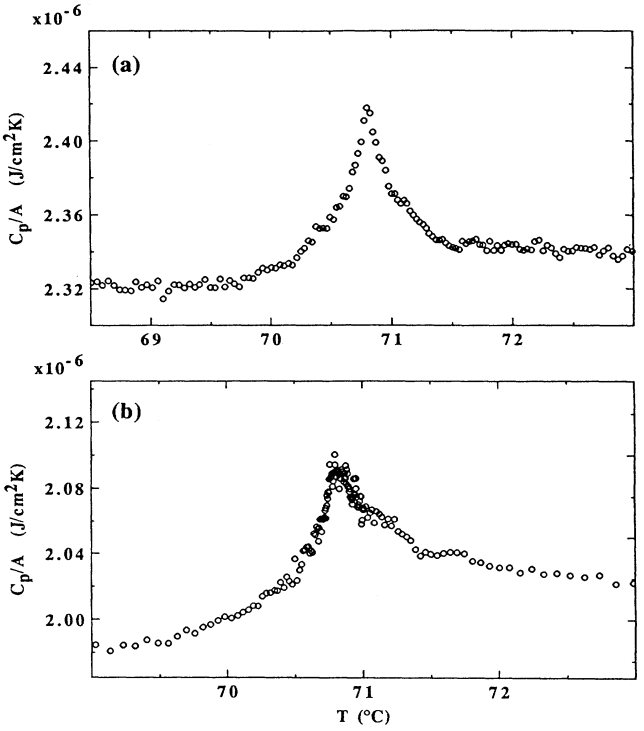

FIG. 12. Heat-capacity data in the vicinity of the AB_s transition for (a) eight- and (b) six-layer 75OBC films.

B. Heat-capacity data for surface liquid-hexatic transitions

The AB_s transitions in Fig. 6 can be considered as an example of 2D hexatic ordering on a liquid substrate. This transition was studied as a function of decreasing film thickness. Heat-capacity data for the surface liquid-hexatic transitions of eight- and six-layer 75OBC films are shown in Fig. 12. Similar data appear in Fig. 13 for four- and three-layer films.

The data in Figs. 12 and 13 are quite similar. All are asymmetric anomalies exhibiting an increased background above the transition. To within the errors present in calibrating absolute units for the heat capacities of the various film thicknesses (outlined above) the peaks are the same height. This agrees with the assumption that only the surface layers participate in this transition.

Heat-capacity data for a two-layer 75OBC film are shown in Fig. 14. The difference in background heat capacities is similar to the previous data, although the peak is noticeably sharper. There is also a small upward shift in the transition temperature. The peak height is close to the height of the surface transitions observed in the eight-, six-, four-, and three-layer data. This is a strong confirmation that the fluctuations contributing to these heat-capacity peaks are primarily from hexatic ordering in the surface layers only. Heating and cooling experimental runs of two-layer films yield the same heat-capacity anomaly without thermal hysteresis to within our experimental resolution (approximately 4 mK). Experimental efforts to investigate the origin (intrinsic or systematic) of the difference in background heat capacity between $T > T_{AB_s}$ and $T < T_{AB_s}$ are in progress.

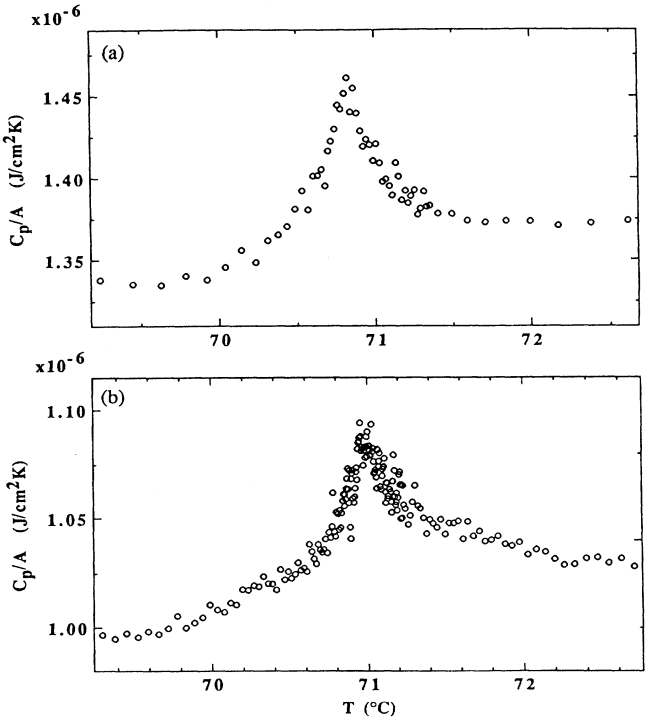

FIG. 13. Heat-capacity data near the AB_s transition for (a) four- and (b) three-layer 75OBC films.

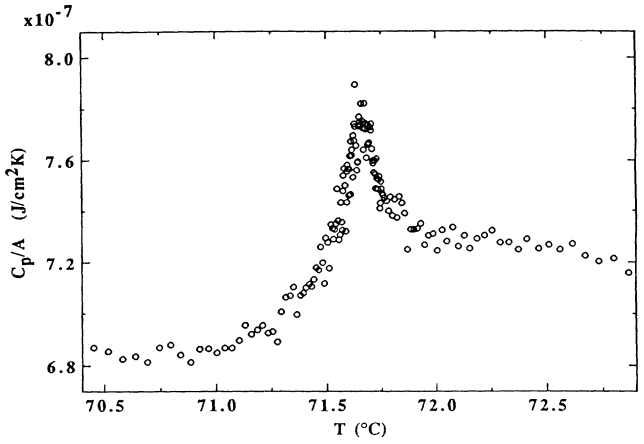

FIG. 14. Heat-capacity data in the neighborhood of the Sm-A–Hex-B transition for two-layer 75OBC films.

C. Heat-capacity data for interior liquid-hexatic transitions

The similarity of the surface transitions for the various film thicknesses discussed above implies little thickness dependence. To address this issue for the AB_{AS} and AB_i transitions, heat-capacity data near these transitions for various film thicknesses are shown in Figs. 8, 15, and 16.

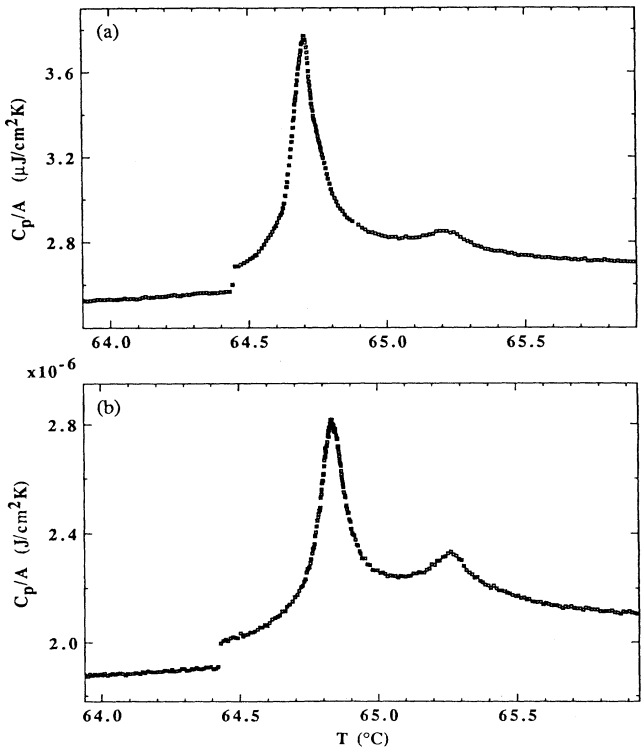

FIG. 15. Heat-capacity data near the AB_{AS} and the AB_i transitions for (a) nine- and (b) seven-layer 75OBC films. The surface Hex-B–Cry-E transition jumps are clearly evident for both films.

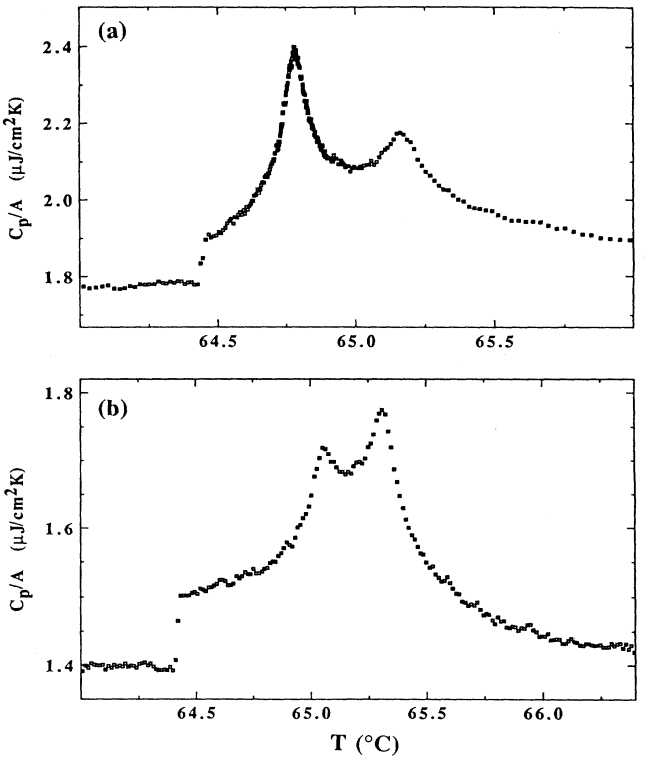

FIG. 16. Heat-capacity data in the vicinity of the AB_{AS} and the AB_i transitions for (a) six- and (b) five-layer 75OBC films.

These data verify the interpretation of the x-ray and electron-diffraction data. The appropriate heat-capacity data for nine- and seven-layer films are displayed in Fig. 15. The peak associated with the AB_{AS} transition is relatively more pronounced in the seven-layer data as there are two less interior layers than for the data in Fig. 15(a). The surface-hexatic–Cry-E transition jumps can be seen below the AB_i transitions.

Figure 16 shows six- and five-layer film data. Note that in the six-layer film data approximately two layers participate in each of the three Sm-A–Hex-B transitions [see Fig. 12(b) for the six-layer AB_s transition data]. However, the innermost transition peak is significantly larger than the other two. This is also evident for the data in Figs. 15(a) and 15(b) wherein the interior transition peak results from the ordering of five and three layers, respectively. It is clear that the interior peak removes a greater entropy/layer than the AB_s or AB_{AS} peaks. At present there is no simple explanation for this other than the development of correlations between the hexatic order of the surface layers which accompanies the interior hexatic transition (although intuitively such a reduction of entropy would be fairly small). Perhaps the local positional order is also increased as the hexatic order extends between layers at the interior transition. Such positional order, although short range, is responsible for much of the entropy release in the bulk liquid-hexatic transitions.

For five-layer films, only the innermost layer partici-

pates in the lowest-temperature transition. The corresponding heat capacity peak is smaller than that of the AB_{AS} transition. The fact that two separate liquid-hexatic peaks from adjacent layers can exist so closely in temperature emphasizes the anisotropic nature of these smectic films. Even though correlations of hexatic fluctuations are large near the AB_{AS} transition, the interlayer coupling is sufficiently weak to prevent a preemptive transition in the innermost layer. The existence of such distinct layer transitions in these films is one of the most unique features of this research. Following this reasoning, one expects that for four-layer films only a single interior transition is expected. This is indeed the case as shown in Fig. 8(a). The singular nature of the AB_{AS} transition heat capacity peak of the four-layer (as well as five-layer) data will be analyzed quantitatively in Sec. IV B. For a three-layer film the AB_{AS} transition is still present but the heat capacity peak is severely diminished. The reduction in peak height (by a factor of 5.3) is considerably greater than the factor of 2 naively anticipated. The decreased peak height is most likely due to the strong ordering effects of the surfaces. Still, the surface effects are not large enough to preempt the interior transition entirely.

The evolution of the liquid-hexatic peaks in Figs. 8 and 16 unambiguously confirm the interpretation of the diffraction data concerning the hexatic ordering of the films. The relative magnitudes and widths of the heat capacity peaks in Fig. 7 have interesting implications on the nature of liquid-hexatic transitions in free-standing films which will be discussed in Sec. IV B.

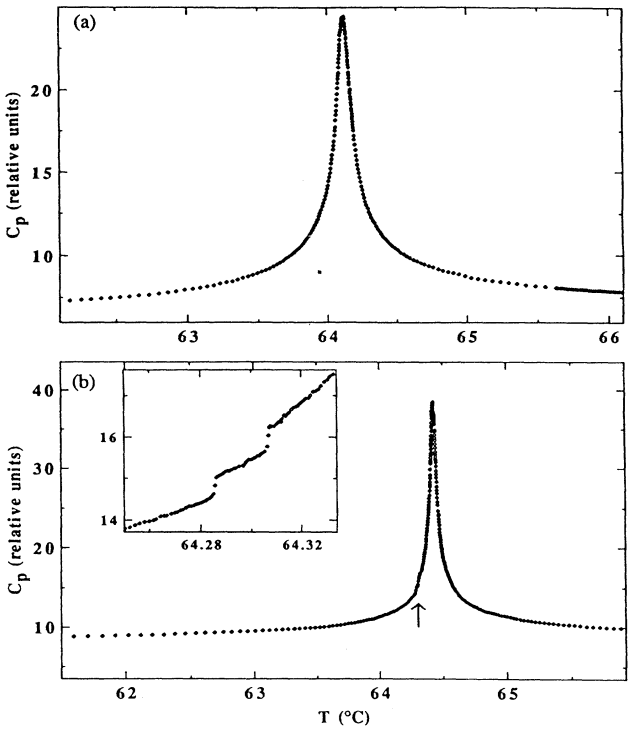

FIG. 17. Heat-capacity data near the AB_i transition for (a) 300- and (b) 130-layer 75OBC films. The inset in (b) shows greater detail near abrupt jumps in the heat capacity associated with the surface Hex-B–Cry-E transition for the 130-layer film.

D. Effects of surface Cry-E order on the interior liquid-hexatic transition

The liquid-hexatic transitions discussed above were nonhysteretic. The surface Hex-B–Cry-E transition, however, is strongly first order with a large thermal hysteresis. This leads to very unique behavior in connection with the interior Sm-A–Hex-B transition. Figure 17(a) shows the heat capacity of a thick (> 300 layers) 75OBC film. In principle, there should be a surface-Hex-B–Cry-E transition below the peak temperature. Currently, our calorimeter fails to detect the corresponding heat capacity jump in very thick films. A surface-Hex-B–Cry-E transition can be resolved for a 130- ($\pm$10) layer film [see Fig. 17(b)]. These data were taken in a cooling run. A series of experiments were conducted to study the nature of this transition. Some of the heat-capacity results are displayed in Fig. 18. The data were obtained from both cooling and heating runs. The film thicknesses (in number of molecular layers) are (a) 70, (b) 26, (c) 13, and (d) 9, respectively. The fact that the heat-capacity data show both thermal hystereses between the cooling and heating runs and sharp heat capacity jumps implies that the relevant transition is strongly first order. In the thick films (> 300 layers), we would not detect any thermal hysteresis. The experimental results from electron-diffraction [5,33] and heat-capacity measurements [34] on three-layer films point to the fact that this is the Hex-B–Cry-E transition occurring at two surface layers of the free-standing films. Actually, Fig. 18 shows a very unique and interesting interplay between the first-order surface-Hex-B–Cry-E transition and the continuous interior Sm-A–Hex-B transition. The salient point is that upon cooling the heat capacity jump occurs at a temperature slightly below the interior Sm-A–Hex-B transition temperature (T_{AB_i}) and upon heating the jump is found at a temperature above T_{AB_i}. The most striking feature of this unique hysteretic effect is that the heat-capacity anomaly associated with the AB_i transition is drastically suppressed and its magnitude decreases as the film thickness decreases to nine molecular layers. Other films with intermediate thickness (e.g., 20- and 40-layer films) yield similar results.

Due to the effects of the free surfaces, the T_{AB_i}'s for thin films increase with decreasing layer number. The surface Hex-B–Cry-E transition temperatures do not share this behavior. For sufficiently thin films the AB_i transition occurs at a higher temperature than the melting of the surface crystal phase. This is the case for the seven-layer data in Fig. 19. The surface crystal melts just below the T_{AB_i}. The origin of the small dip in the seven-layer heating data just before the melting of the surface crystal is unknown. Similar features are often seen for other first-order transitions. Following the melting of the surface Cry-E phase the heating data in Fig. 19 fall nicely on the cooling data. There is only a slight hysteresis (the

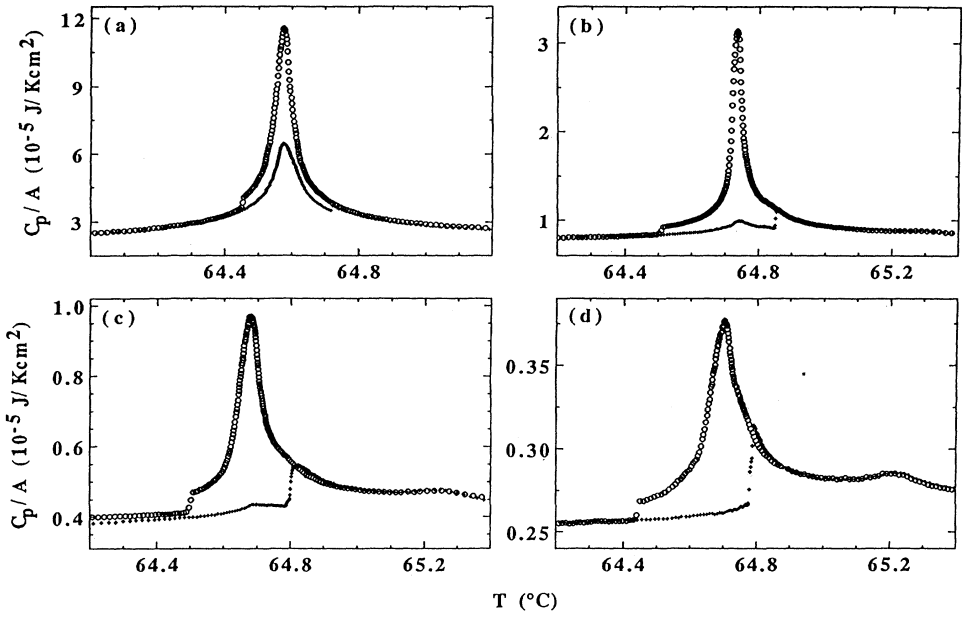

FIG. 18. Heat-capacity data near the AB_i transition obtained from both heating and cooling scans of (a) 70-, (b) 26-, (c) 13-, and (d) 9-layer 75OBC films.

heating peak temperature is 6 mK greater than that of cooling), which is surprising considering the surface crystal phase melts just 24 mK below the heat capacity peak of the AB_i transition.

The most impressive feature of the data presented in Fig. 18 is the depression of the interior Sm-A–Hex-B heat-capacity peak in the presence of the surface-Cry-E phase. This corresponds to a reduction of the enthalpy release through this transition. Since the system enthalpy is a state variable it is independent of the thermodynamic path between the surface Cry-E interior-Hex-B phase and the Sm-A phase. Thus the enthalpy difference ΔH between these two phases is the same for cooling or heating. This requires that the enthalpy corresponding to the area between the heat-capacity curves for cooling and heating be equal to the difference in latent heats, L_{melting}-L_{freezing}, of the surface-Hex-B–Cry-E transition. Unfortunately, since our heat-capacity measurement relies on an ac technique, no measurement of the latent heats associated with the first-order surface-Hex-B–Cry-E could be made to check this equality. Figure 20(a) shows a plot of the difference in areas under the heat-capacity curves for heating and cooling as a function of layer thickness. From the argument above, this area is proportional to the additional latent heat released in the melting of the surface Cry-E layers. Figure 20(b) plots the same data nor-

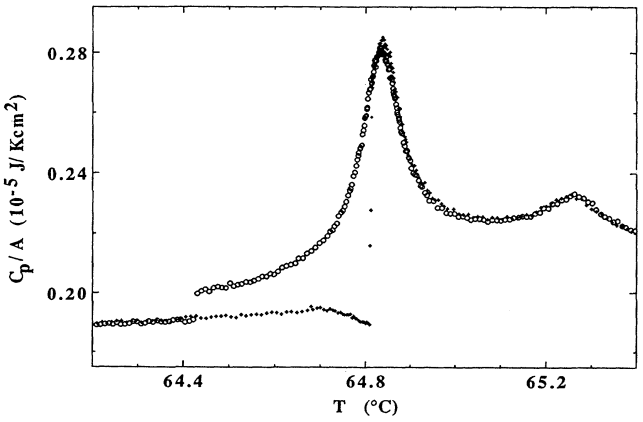

FIG. 19. Heat-capacity data in the vicinity of the AB_i transition obtained from both heating and cooling runs of a seven-layer 75OBC films.

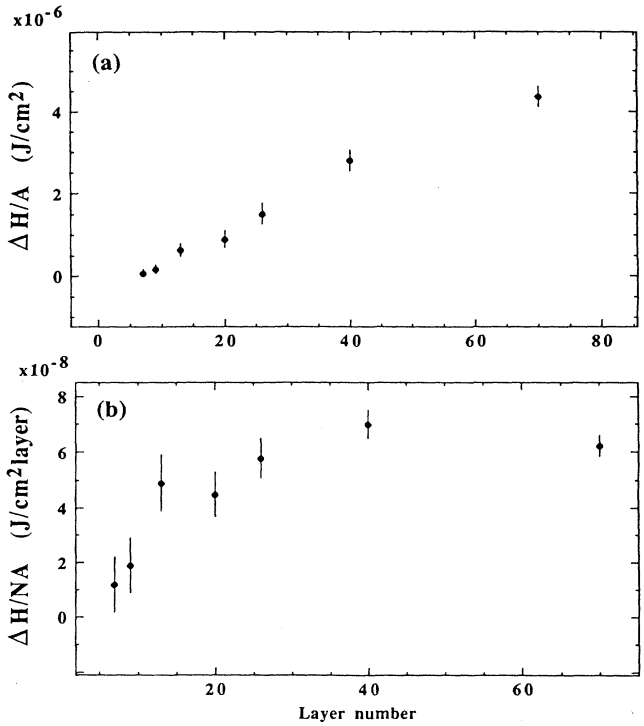

FIG. 20. (a) $\Delta H/A$ and (b) $\Delta H/NA$ vs layer number (N).

malized by layer number (N). The sudden drop as N approaches seven coincides with the upward shift of the interior Sm-A–Hex-B transition temperatures.

The depression of the Sm-A–Hex-B heat-capacity peak in the presence of surface-Cry-E layers leads to two interpretations. (1) The surface-Cry-E phase induces stronger positional order in the interior Sm-A phase, i.e., the difference in the positional correlation lengths between the Hex-B and Sm-A phases (both of which possess exponentially decaying positional correlations) is smaller, leading to a lower entropy release. (2) The surface-Cry-E phase induces hexatic order in the layers adjacent to the surface which do not participate in the melting of the interior-Hex-B layers, hence lowering the entropy release. These "near-surface" hexatic layers would melt along with the surface-Cry-E layers. Both scenarios imply a characteristic penetration depth for the effects of the Cry-E surfaces, resulting in a maximum for the layer normalized entropy difference $\Delta S/N$ at some intermediate thickness. This is plotted in Fig. 20(b). Although the data are not conclusive, a maximum can be seen at 40 layers. From the heat-capacity data alone it is not possible to differentiate between the above scenarios as to the origin of the decreased entropy release of the AB_i transition in the presence of surface Cry-E layers. It is worth noting that while the amplitudes of the aforementioned Sm-A–Hex-B peaks are severely depressed, the transition temperatures are virtually unchanged from the values observed in cooling data.

To determine thermal hysteresis of the AB_i transition for 75OBC films thicker than six layers, runs were conducted in which the film was not cooled below the surface-Hex-B–Cry-E transition. These runs were also performed to see if the occurrence of the surface-Cry-E phase below the AB_i transition was due to a supercooling effect, i.e., if the film would spontaneously develop a surface-Cry-E phase once the ramping rate was reversed at any temperature below that where the surface crystal phase melts on heating. Figure 21 shows detailed heating and cooling data for a ten-layer 75OBC film. The reproducibility between heating and cooling is excellent. The inset shows conclusively the lack of hysteresis in the AB_i transition temperature. The temperature scanning rates used in obtaining this data varied between 0.5 and 3 mK/min. Before the rate was reversed, the film was maintained at 64.6 °C for approximately 1 h to check for spontaneous formation of a surface phase.

E. Thickness dependence of liquid-hexatic and hexatic-crystal transition temperatures

Thickness dependence of phase transition temperatures is seen in a variety of liquid-crystal systems (see Sec. I) and 75OBC exhibits similar behavior. As the films become thinner, effects due to the free surfaces, which possess some characteristic decay length (or penetration depth), become apparent in the evolution of the transition temperatures. The transition temperatures for the liquid-hexatic transitions for films between two and ten layers in thickness are presented in Fig. 22. The AB_s transition temperatures are approximately constant for $N \geq 3$. Similar behavior is seen in the AB_{AS} transitions for $N \geq 5$. Note that the sudden increases in the AB_s and AB_{AS} transition temperatures first occur when the layers participating in the transition are adjacent to one another. For the AB_s transition this is only the case for a two-layer film. However, it occurs for the AB_{AS} transition at four layers. These sudden increases in transition temperatures are most likely due to an increase in the hexatic order from the direct interlayer coupling. Similar effects raise the transition temperature of the three-layer AB_{AS} transition.

The AB_i transition temperatures in Fig. 22 show a small but noticeable rise for films less than eight layers thick. Note that the increases in the AB_i transition temperatures in the films result not only from the effects of the free surfaces, but also may be due to the presence of hexatic order in the layers near the surface which may act as an external hexatic field. The latter is an indepen-

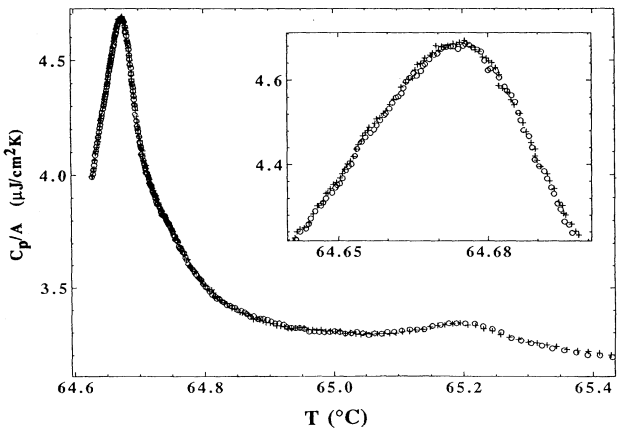

FIG. 21. Heat-capacity data from cooling and heating scans of a ten-layer 75OBC film in the vicinity of the AB_{AS} and AB_i transitions. Inset shows the detail near the AB_i peak. The reproducibility between heating and cooling is excellent. The film was kept above 64.6 °C to avoid the surface Cry-E phase.

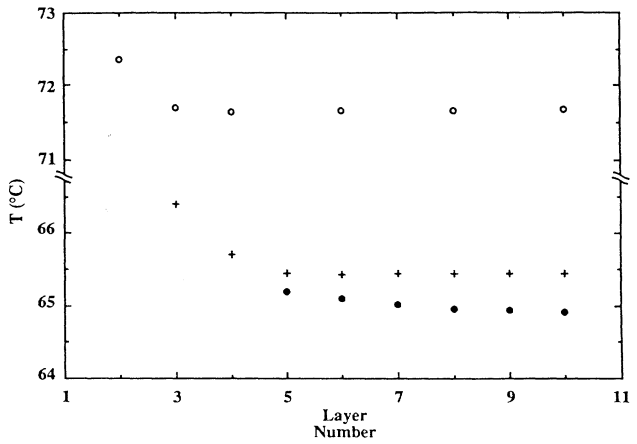

FIG. 22. Transition temperatures for thin 75OBC films. Open circles (crosses) denote the AB_s (AB_{AS}) transitions. The AB_i transition temperature are represented by solid circles.

dent effect not due to the presence of free surfaces, but rather from the surface hexatic order. In the presence of such an ordering field the transition would become first order, analogous to the paramagnet-ferromagnet transition in an external magnetic field. The lack of thermal hysteresis in the AB_i and AB_{AS} transition temperatures for the data in Fig. 21 implies that effects of the surface hexatic order are relatively minor.

Up to this point, this section has examined the behavior of liquid-hexatic transition temperatures only for thin films and the above data have concentrated on the influence of the free surfaces. As the system moves away from the two-dimensional limit, finite-size effects are expected to play a role. Unfortnately, the proximity of the surface-hexatic-crystal and surface-liquid-hexatic transitions to the interior heat capacity peak make detailed fitting impossible with a reasonable number of parameters. The transition temperatures for thicker films, however, are accessible. Since the incident laser power and film absorption were calibrated for films of 75OBC it was possible to determine the temperature offset induced by the laser heating. It was determined empirically by scanning through the Sm-A–Hex-B phase transition, attenuating the laser beam with a neutral density filter, and repeating the scan. For a ten-layer 65OBC film, attenuating the beam by 30% produced a T_{AB_i} shift of 66 mK, implying a dc temperatre offset of approximately 22 mK/layer (24 mK/layer for 75OBC). The data scans previously shown in this section have not been corrected for this, but plots of transition temperatures versus thickness have. Sample deterioration and transition temperature shifts were also monitored. Particular films showed negligible downward T_{AB_i} shifts (3–5 mK/day), and transition temperatures were very consistent from film to film. Consequently, none of the temperature scales have been corrected for such shifts. Figure 23 shows AB_i transition temperatures as a function of thickness from 3 to 70 layers. Finite-size effects are responsible for the slow rise towards higher values of N (as discussed below). The inset shows the melting temperature of the surface-Cry-E phase as it crosses the AB_i phase boundary.

Finally, transition temperatures associated with the surface-Hex-B–Cry-E transition are presented. Figure 24(a) shows the temperatures at which the jumps are observed in the heat capacity for heating and cooling data. The dependence of film thickness for these temperatures is much noisier than that of the liquid-hexatic transitions, due to the first-order nature of this transition. In spite of this, a clear downward trend is observed with decreasing layer number. Since this transition occurs on the surfaces of the film it does not experience a 3D-2D crossover in the conventional sense. It is more likely that surface effects limit the spatial fluctuations of Cry-E domains for thinner films, reducing the probability of nucleation and hence decreasing the transition temperature. Figure 24(b) plots the thermal hysteresis associated with the surface-Hex-B–Cry-E transition. There is an overall decrease with increasing layer thickness, with the exception of a sharp dip centered near thirteen layers. The origin of this feature is unknown, although it should be pointed out that 13 layers is precisely the thickness below which the AB_i transition heat-capacity anomaly can no longer be resolved on heating.

The interior-Hex-B–Cry-E transition occurred near

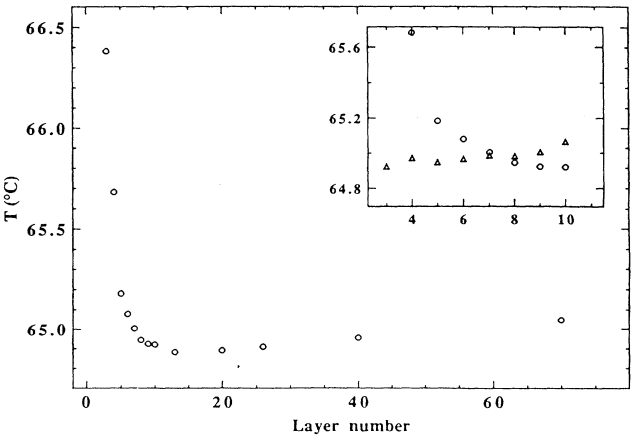

FIG. 23. The AB_i transition temperatures as a function of thickness for 75OBC films. The inset shows the melting temperature of the surface Cry-E phase (triangles) as it crosses the AB_i phase boundary (circles).

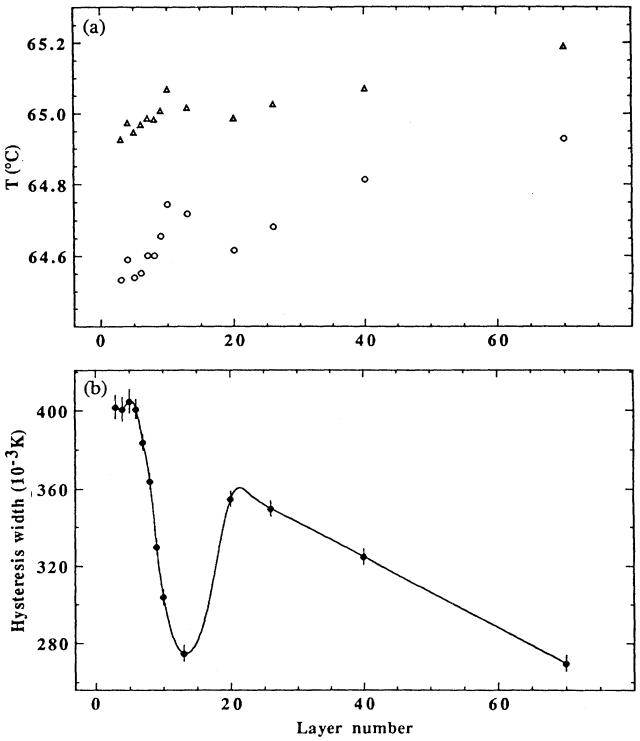

FIG. 24. (a) Melting (triangles) and freezing (circles) temperatures for the surface Cry-E phase. A downward trend is apparent. (b) Thermal hysteresis width for the surface Hex-B–Cry-E transition. The origins of the hysteresis dip near 13 layers and the overall decrease with increasing N are not understood at this time. The solid line in (b) is a guide to the eye.

59.7 °C for all of the thick films studied. Thinner films often broke at these temperatures. It is possible that the large density discontinuity at the Hex-B–Cry-E phase induces a strain great ehough to rupture the film. The interior-Hex-B–Cry-E transition was recorded for 7-, 10-, and 13-layer films. These transition temperatures were all within 20 mK of 59.65 °C. The interior-Hex-B–Cry-E hysteresis width measured for 50- and 130-layer films was 370±8 mK, very close to the value of 381 mK determined from bulk measurements of 75OBC.

IV. DISCUSSION AND ANALYSIS

A. Surface and two-layer liquid-hexatic transitions

The heat capacities near the AB_s transitions, shown in Figs. 12–14, bear some resemblance to the predicted shape of the heat-capacity anomaly for the 2D XY model (Fig. 1). It is impossible to accurately compare the peak widths due to the ambiguity in the temperature scales, however. In Fig. 1 an absolute temperature scale is used in units of the spin-spin coupling constant and the hexatic phase is the zero-temperature ground state of the system in that calculation (certainly not the case for the free-standing films). The analogous coupling constants for the hexatic liquid-crystal films have not been determined. Further exerimental investigations are in progress to determine the origin of the difference in the background heat capacity between $T > T_{AB_s}$ and $T < T_{AB_s}$.

B. Interior liquid-hexatic transitions

The heat-capacity data for the surface liquid-hexatic transition possessed a signal to noise ratio which prohibited meaningul fitting (although the calorimetric system is being continually improved). The quality of the data on the interior transitions in four- and five-layer films allowed successful fitting, however (the surface-Hex$B$–Cry-E transition was also far enough away to give a reasonable fitting range). The singular appearance of these peaks suggested fitting to power-law expressions. The Marquardt algorithm was employed for the nonlinear least-squares fitting routine. Thick-film data (Fig. 5) were weighted according to the propagation of instrumental error in determining the heat capacity. Results using this, versus no weighting of the data, did not vary significantly. The noise in the thin film data made the effects of weighting immaterial. The quality of the fits were determined from the χ^2 values defined by

$$\chi^2=\Phi^2/(N_d-p) ,$$

where Φ^2 are the squared differences between the fit and the data, N_d is the number of data points being fitted, and p is the number of fitting parameters varied. Uncertainties for specific parameters were determined for the thick film results by fixing all other parameters and varying the parameter of interest until the χ^2 value doubled. The expressions used to fit the heat-capacity data correspond to those used in Ref. [31],

$$C_p=\begin{cases} A^+|t|^{-\alpha}(1+E^+|t|^x)+B+Dt, & T>T_c \\ A^-|t|^{-\alpha}(1+E^-|t|^x)+B+Dt, & T<T_c . \end{cases} \quad (12)$$

The scaling correction terms ($E^{\pm}|t|^x$) are included to account for departures from the asymptotic scaling behavior and ensure a smooth variation of the background through T_c. Although always present in the fitting expression for the thick-film data of Fig. 5 [27], the correction to scaling terms were not used initially in the fits for the thin film data. Figure 25 shows fitting results from one set of 75OBC four-layer data. The fit to these data converged to a singularity, i.e., $\alpha>0$. The value of α (=0.28) obtained from the fit was very stable. The noise present in the thin film data complicated χ space giving rise to several local minima. Fits were always checked by incrementally stepping the fitted temperature range to larger or smaller values. Once an upper or lower range was reached the procedure was reversed to see if the fits were converging to another minimum in χ space. The fits in Fig. 25 were very stable between fitting windows of ±1.2 and ±0.1 K. Fits extended over one and a half decades from $|T-T_c|=25$ mK to $|T-T_c|=1.2$ K.

To improve the fits far away from the transition in the four-layer film data, correction to scaling terms were included after the value of α had been determined. This was done only for the largest fitting windows. These terms had negligible effects on α and the amplitude ratio A^+/A^-. The relative contributions of the correction to scaling terms was less than 2% at one decade, and was never larger than 8%.

Five-layer 75OBC data were also fitted using the following expression:

$$C_p=\begin{cases} A^+|T-T_1|^{-\alpha}+B^+|T-T_2|^{-\alpha}+B, & T>T_1 \\ A^-|T-T_1|^{-\alpha}+B^+|T-T_2|^{-\alpha}+B, & T_2>T<T_1 \\ A^-|T-T_1|^{-\alpha}+B^-|T-T_2|^{-\alpha}+B, & T<T_2 . \end{cases} \quad (13)$$

This is simply an expression for two superposed power-law singularities. The resulting fit, shown in Fig. 26, yields $\alpha=0.27\pm0.04$. This is in very good agreement with the four-layer 75OBC fits and further supports the

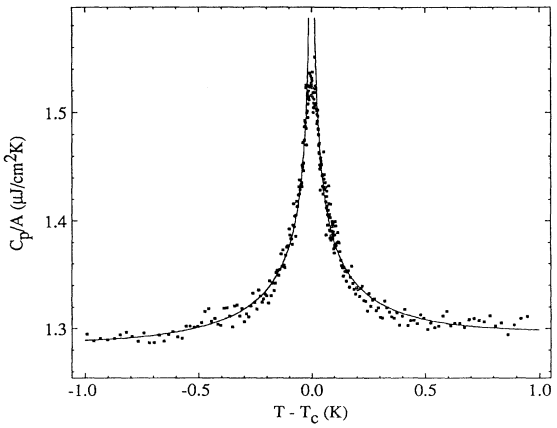

FIG. 25. Fitting results (solid line) to the heat-capacity anomaly from the interior layers of a four-layer 75OBC film. The fitting parameters are $\alpha=0.28\pm0.04$, $A^+/A^-=0.94\pm0.03$, $E^+/E^-=1.65\pm0.05$, and $E^+/A^+=0.03$.

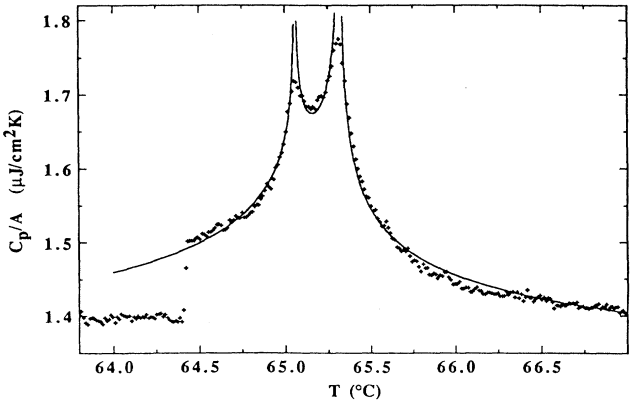

FIG. 26. Heat capacity and fit results of both the AB_{AS} and AB_i transitions from a five-layer 75OBC film. The fitting parameters are $\alpha=0.27\pm0.04$, $A^+/A^-=0.80\pm0.03$, $B^+/B^-=1.04\pm0.05$, and $A^+/B^+=1.49$.

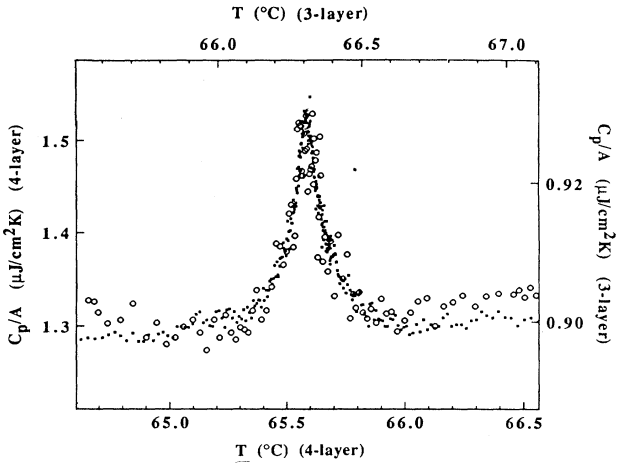

FIG. 27. Overlay of heat capacities near the AB_{AS} transitions for four-layer (solid dots) and three-layer (open circles) 75OBC films. Although the three-layer data are noisy, there is no resolvable change in the width of the peak. The three-layer data have been expanded by a factor of 5.3.

values of α for that data. This also suggests that, aside from the size and position of the peak, the interior liquid-hexatic and AB_{AS} transitions at these thicknesses possess essentially the same critical properties. Due to the small temperature window available for fitting, the value of α was not allowed to differ for the two peaks.

The singular nature of the interior four- and five-layer liquid-hexatic transitions is very puzzling. It is generally accepted that a heat-capacity singularity associated with a continuous phase transition will become a broadened, finite anomaly in an external ordering field. This is the usual explanation given for the heat-capacity peak of the Sm-C–Sm-I transition in bulk liquid-crystal compounds which is much broader than the corresponding Sm-A–Hex-B heat-capacity peaks. In this case the external field is the tilt field of the Sm-C phase. Such broadening is contrary to the data of Fig. 8. The interior transitions are significantly sharper for the four- and three-layer heat-capacity data. At present we are investigating this important feature carefully. Theoretically, one may consider a system of coupled 2D XY layers. The unbinding of disclination pairs in the interior of the five-, four-, and three-layer films takes place in a layer (or layers) which is weakly coupled to layers in which disclination pairs are still bound. If the interaction of disclinations between layers is attractive the bound pairs may alter the divergence of the 2D XY correlation length (the length between free disclinations). If the divergence becomes power-law-like, the heat capacity may develop a singular appearance. It would be interesting to perform renormalization-group calculations or numerical simulations to see if such a scenario is possible. An alternative scenario concerning the presence of herringbone fluctuations is discussed below.

The heat-capacity data of the three-layer AB_i transition was too noisy for a meaningful fit. To compare this data to the four-layer results the scale of the former was increased by a factor of 5.3 and superimposed on the four-layer peak. This is shown in Fig. 27. The peaks are essentially the same (apart from the scale factor). There is no increase in width, which is unexpected since the interior layer in a three-layer film experiences a stronger hexatic field due to the surface hexatic order and has a higher transition temperature. A similar overlay appears in Fig. 28 for the AB_{AS} transition of a ten-layer film and the four-layer data of Fig. 25. A smooth background determined from fits to the high-temperature side of the ten-layer data was subtracted from the surface transition. In this case there is no dilation of scales since both peaks result from the ordering of two layers. The ten-layer AB_{AS} peak is broader and slightly smaller. The in-

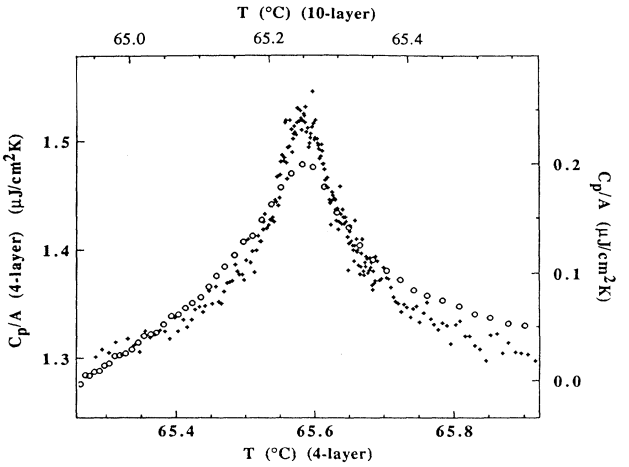

FIG. 28. Overlay of heat capacities near the AB_{AS} transitions for four-layer (crosses) and ten-layer (open circles) 75OBC films. The zero for the ten-layer data is set relative to a smooth background determined by fitting the ten-layer interior Sm-A–Hex-B heat-capacity peak. The width of the heat capacity and temperature windows, however, are the same for both sets of data. The ten-layer peak is slightly smaller and broader than that of the four-layer film.

creased width of the ten-layer AB_{AS} peak is consistent with the behavior exhibited by the AB_s transitions. The peaks resulting from ordering of adjacent layers are sharper than for layers which are separated by liquid layers.

C. Speculation on alternatives to the 2D *XY* theory

Although the surface liquid-hexatic transition data qualitatively resemble 2D *XY* model calculations for the heat capacity, their appearance is far more singular than can be accounted for by theory. There is also no reason to expect that the Kosterlitz-Thouless theory completely describes this transition, although this is the only theory yielding a continuous phase transition for the 2D *XY* model. If the heat capacity is assumed to be singular, two possible explanations are multicriticality or the influence of non-2D *XY* fluctuations.

Multicriticality. From the work by Berker and Nelson [19] there exists no tricritical point in the 2D ^{3}He-^{4}He phase diagram in that the normal-superfluid transition line never intersects the tip of the coexistence curves. The approach is arbitrarily close for certain values of the interaction parameters. Thus multicriticality for a 2D *XY* system cannot be ruled out. A different kind of crossover exists in the Halperin-Nelson model for different values of the dislocation core energy E_c. Numerical studies quoted in Sec. I C point to a first-order 2D crystal-liquid transition for small values of the core energy. Such a transition preempts the hexatic phase entirely. If the disclination core energy E_{cd} is decreased, a similar discontinuous hexatic-liquid transition may exist. However, the value of E_{cd} is nontrivially related to E_c and it is not known if the values of E_{cd} resulting in a first-order, or weakly first-order, liquid-hexatic transition would lead to a stable hexatic phase. More detailed work on critical phenomena in 2D *XY* systems is required before these possibilities can be considered.

Presence of non-2D XY fluctuations. The existence of a surface-Hex-*B*–Cry-*E* transition so close to the Sm-*A*–Hex-*B* transitions confirms the presence of herringbone orientational ordering in this system and implies a possible coupling between hexatic and herringbone order parameters. This influence was considered in detail for 3D Sm-*A*–Hex-*B* phase transitions [35]. It was demonstrated in Ref. [36] that herringbone packing can exist on a distorted hexagonal lattice in three distinct configurations. None of these can be transformed to another by any combination of lattice translations. Thus the order parameter between a plastic crystal (no local molecular orientational order) and a phase possessing herringbone packing is that of a three-state Potts model. Bruinsma and Aeppli [35] argue that since translational order is not present in hexatic phases, local herringbone order is represented by another *XY*-like order parameter. However, herringbone order has been observed in hexatic phases [4]. This leads to herringbone order-parameter fluctuations which possess the three-state Potts symmetry. Such fluctuations may dominate the heat capacity near the transition. This would be consistent with the value of α obtained from the fits on four- and five-layer films since the heat capacity of the 2D three-state Potts model diverges with $\alpha=\frac{1}{3}$.

D. Transition temperatures

Normally, the temperature for an order/disorder transition decreases in a lower dimension (assuming the ordered phase is stable in that dimension). The crossover from 3D to 2D behavior in liquid-crystal free-standing films, however, is complicated by the enhancement of order at the free surfaces. In the 75OBC films the presence of free surfaces increases the liquid-hexatic transition temperatures as the layer number is reduced. Even for two-layer films the layer-layer interaction energy may play a role in increasing the liquid-hexatic transition temperature. However, there is no reason to expect that such effects will necessarily alter the 2D nature of these transitions.

The appearance of a surface ordering transition can be shown using mean field theory as in Ref. [15]. This theory treats surface critical phenomena, for the most part, in the semi-infinite limit. The surface transition temperature is determined uniquely by the surface energy (proportional to λ^{-1} where λ has units of length) and the bulk correlation length ξ_b. For a finite number of layers, the film thickness L also determines the surface transition temperature [see Eq. (6)]. Assuming $\xi_b(T) = \xi_0|(T-T_c)/T_c|^{-\nu}$ ($\nu=1/2$), λ and ξ_0 can be used as free parameters to fit Eq. (6) to the measured values for the AB_s transition temperatures. This fit is shown in Fig. 29. The values of λ and ξ_0 determined from this fit are 0.57 and 0.08, respectively (in units of layer spacing). The fit is reasonable, although the freedom of λ and ξ_0 limit its validity. The origin of the small dip near four-layers cannot be described by this simple model.

Notwithstanding the qualitative agreement with the AB_s transition temperatures, the theory does not predict more than one interior transition nor any thickness dependence of the interior transition temperatures. As

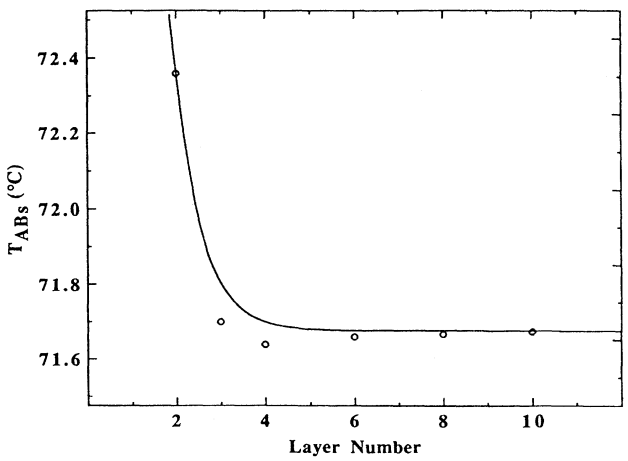

FIG. 29. Transition temperatures for thin 75OBC films and a fit to Eq. (6). The fit yields values for λ and ξ_0 of 0.57 and 0.08, respectively (distances are in units of layers). The fit does not reproduce the minimum near four layers.

mentioned in Sec. I, Heinekamp *et al.* [6] used a variation of this model to fit surface Sm-A–Sm-C transition temperatures determined from order-parameter measurements of DOBAMBC. As in our case, the agreement was only qualitative in nature. To obtain better agreement between mean-field theory and their results, they included a linear temperature dependence in the surface energy. There is little justification for this assumption since finite-size and surface proximity effects must certainly be included before temperature dependence of the surface energy is assumed.

The model of Li *et al.* [16] introduced in Sec. I B employs a more fundamental approach. Their model predicts a crossover between regions dominated by finite-size effects and surface interactions, respectively. This crossover occurs for N close to ξ_s. Specifically, as the layer number N is reduced, the interior transition temperature T_{AB_i} decreases from the $N=\infty$ value, until a minimum is reached. The thickness at which this minimum occurs is defined as ξ_s. For thicknesses below ξ_s the interior transition temperature increases dramatically. Transition temperatures calculated from this model are plotted in Fig. 30 as $T_B(N)-T_B(\infty)$ vs N for several values of the surface coupling constant J_S (for the purposes of this calculation both J_V and J_H were set equal to one). Figure 23 shows interior hexatic transition temperatures as a function of thickness determined from our heat-capacity measurements of 75OBC free-standing films. The qualitative agreement between Figs. 30 and 23 is very good.

The initial decrease of the transition temperatures from the bulk value is consistent with predictions of reduced dimensionality. It is only at length scales below ξ_s that the enhanced surface coupling starts to affect the phase-transition temperatures. From Fig. 23, ξ_s for the Sm-A–Hex-B transition lies somewhere around 20 layers. Bulk behavior is not expected unless $N \gg \xi_s$ and a

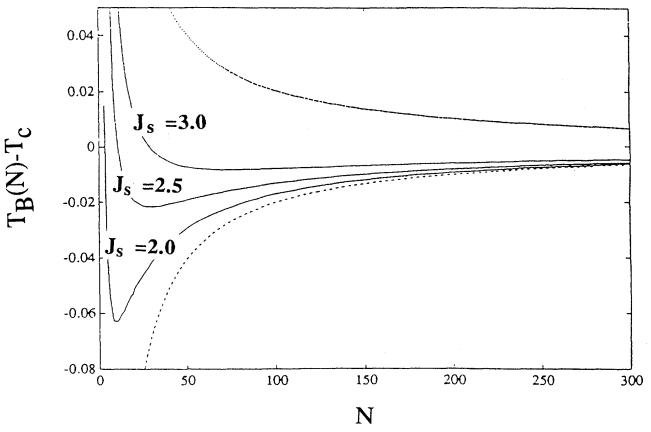

FIG. 30. Plots of transition temperatures as a function of thickness for the 2D Ising strip reported by Li *et al.* [16]. Solid lines correspond to different values of the surface in-plane coupling constant. Dashed and dotted lines are limiting curves for $J_S=0$ and ∞, respectively. Transition temperatures are expressed as the difference between the peak position of an n-layer strip $T_B(n)$ and transition temperature (T_c) of the infinite system.

"surface-dominated" regime only exists for films significantly less than ξ_s. This crossover length may explain certain inconsistencies seen in various measurements of free-standing liquid-crystal films. For example, this research, especially Fig. 22, implies that the free surfaces do not begin to affect the interior liquid-hexatic transitions until N is less than ten layers. Measurements of the tilt order parameter in the Sm-C phase of thin DOBAMBC films present a similar picture of the crossover to the surface dominated regime. There, except for the appearance of a higher-temperature surface-Sm-C transition, order-parameter profiles began to lie on the bulk curve for a ten-layer film. In contrast to this, comprehensive x-ray studies of 7O.7 reveal thickness dependence in the phase diagrams for films as thick as 200 layers. If the simple model presented in Ref. [16] can be applied to these systems, then the aforementioned measurements are simply probing behavior on length scales less than (in the case of this heat-capacity work and the tilt profiles of DOBAMBC) or greater than (the x-ray studies of 7O.7) ξ_s. Comprehensive studies of more realistic models are required to confirm this simple picture.

For comparison with the Ising model results, Li *et al.* [16] also present a mean-field model based on the model used in Ref. [15], part of which was presented in Sec. I B. To adapt this model to the case of layered systems, Li *et al.* [16] calculate the magnetization M_α for each layer. To determine the profile across the film, the couplings to neighboring spins are replaced by effective magnetic fields. Thus the magnetization in each layer is determined by a transcendental equation involving itself and the magnetizations of neighboring layers. These equations are solved self-consistently, yielding the values for M_α. Linearizing the equations which determine the M_α values allows one to determine the behavior of the surface transition as a function of N. From their results Li *et al.* [16] conclude that the surface transition temperature approaches its semi-infinite limit from above, decreasing exponentially with a decay length ξ_s. The AB_s transition temperatures in Fig. 22, however, show a slight drop near four layers. Also, the length scale over which the transition temperatures decay seems to be much shorter than ξ_s. Solving the magnetization equations numerically, the behavior of the interior transition temperature with layer number could also be determined. This is shown in Fig. 30. These transition temperature curves are qualitatively consistent with the experimental data.

In spite of the simplicity of the model, its agreement with the free-standing liquid-crystal heat capacities is impressive. This suggests that the behavior observed in this research may also occur in many other layered systems. Unfortunately, few materials other than liquid crystals tend to exhibit enhanced surface interactions, limiting the number of systems in which this behavior may be found.

V. SUMMARY

A state-of-the-art ac calorimetric system has been constructed in our laboratory. This unique system has a

resolution of about one part in 10^5 in measuring the heat capacity of extremely thin liquid-crystal free-standing films which can be as thin as two molecular layers. Due to the enhancement of order on the surfaces and a relatively weak interlayer interaction, compared with the intralayer interaction, we fail to see the effects of finite-size scaling as the film thickness decreases from a few hundred to two molecular layers. On the other hand, we have discovered several extremely important and interesting physical phenomena, e.g., layer-by-layer surface ordering, competition between the reduced dimensionality and surface ordering effects, criticality near the Sm-*A*–Hex-*B* transition of a two-dimensional film, interplay between the continuous Sm-*A*–Hex-*B* transition and the first-order Hex-*B*–Cry-*E* transition, etc. Further experimental work to obtain more insight into the nature of the Sm-*A*–Hex-*B* and Hex-*B*–Cry-*E* transition in *nm*OBC and other phase transitions between different liquid crystal mesophases (e.g., Sm-*A*–Sm-*C* and Sm-*C*–Sm-*I*) are in progress.

ACKNOWLEDGMENTS

Dr. R. Pindak and Professor J. W. Goodby aided and encouraged our efforts in many ways. Dr. Pindak's experience with measurements on free-standing liquid-crystal films was invaluable, and J. W. Goodby was essential in providing liquid-crystal samples to measure. The oven used in this work was kindly given to us by Dr. R. Pindak. We gratefully acknowledge informative discussions with Dr. D. Bishop, Professor G. Greenlees, Professor J. T. Ho, Professor K. Huang, Professor M. Kardar, Dr. H. Li, Dr. A. Lien, Dr. D. Osheroff, and Professor M. Schick. This work was supported by the Graduate School and the Center of Microelectronic and Information Sciences of the University of Minnesota, the Donors of the Petroleum Research Fund, administered by the American Chemical Society, and the National Science Foundation, Solid State Chemistry, Grants Nos. DMR-84-04945, DMR-85-03419, DMR-89-19334, and DMR-90-24992. Support from the Department of Education (T.S.) and IBM (R.G. and T.S.) is acknowledged.

*Present address: Center for Bio/Molecular Engineering, Code 6090, Naval Research Laboratory, Washington, DC 20375-5000.

[1] C. Y. Young, R. Pindak, N. A. Clark, and R. B. Meyer, Phys. Rev. Lett. **40**, 773 (1978).

[2] R. Pindak, D. J. Bishop, and W. O. Sprenger, Phys. Rev. Lett. **44**, 1461 (1980).

[3] R. Pindak, W. O. Sprenger, D. J. Bishop, D. D. Osheroff, and J. W. Goodby, Phys. Rev. Lett. **48**, 173 (1982).

[4] R. Pindak, D. E. Moncton, S. D. Davey, and J. W. Goodby, Phys. Rev. Lett. **46**, 1135 (1981).

[5] R. Geer, T. Stoebe, C. C. Huang, R. Pindak, G. Srajer, J. W. Goodby, M. Cheng, J. T. Ho, and S. W. Hui, Phys. Rev. Lett. **66**, 1322 (1991).

[6] S. Heinekamp, R. A. Pelcovits, E. Fontes, E. Y. Chen, R. Pindak, and R. B. Meyer, Phys. Rev. Lett. **52**, 1017 (1984).

[7] S. M. Amador and P. S. Pershan, Phys. Rev. A **41**, 4326 (1990).

[8] D. R. Nelson and J. M. Kosterlitz, Phys. Rev. Lett. **39**, 1201 (1977).

[9] E. B. Sirota, P. S. Pershan, S. Amador, and L. B. Sorenson, Phys. Rev. A **35**, 2283 (1987).

[10] S. Amador, P. S. Pershan, H. Stragier, B. D. Swanson, D. J. Tweet, L. B. Sorenson, E. B. Sirota, G. E. Ice, and A. Habenschuss, Phys. Rev. A **39**, 2703 (1989).

[11] J. D. Brock, D. Y. Noh, B. R. McClain, J. D. Litster, R. J. Birgeneau, A. Aharony, P. M. Horn, and J. C. Liang, Z. Phys. B **74**, 197 (1989).

[12] D. J. Tweet, R. Holyst, B. D. Swanson, H. Stragier, and L. B. Sorenson, Phys. Rev. Lett. **65**, 2157 (1990).

[13] S. Gierlotka, P. Lambooy, and W. H. de Jeu, Europhys. Lett. **12**, 341 (1990).

[14] M. Pomerantz and A. Segmuller, Thin Solid Films **68**, 33 (1980).

[15] K. Binder, *Phase Transitions and Critical Phenomena,* edited by C. Domb and J. L. Liebowitz (Academic, London, 1986), Vol. 8.

[16] H. Li, M. Paczuski, M. Kardar, and K. Huang, Phys. Rev. B **44**, 8247 (1991).

[17] B. I. Halperin and D. R. Nelson, Phys. Rev. Lett. **41**, 121 (1978); D. R. Nelson and B. I. Halperin, Phys. Rev. B **19**, 2457 (1979).

[18] J. M. Kosterlitz and D. J. Thouless, J. Phys. C **6**, 1181 (1973).

[19] A. N. Berker and D. R. Nelson, Phys. Rev. B **19**, 2488 (1979).

[20] S. Solla and E. K. Riedel, Phys. Rev. B **23**, 6008 (1981).

[21] Masuo Suzuki, in *Physics of Low Dimensional Systems,* Proceedings of Kyoto Summer Institute, edited by Y. Nagaoka and S. Hikami (Progress of Theoretical Physics, Kyoto, 1979).

[22] D. M. Ceperley and E. L. Pollock, Phys. Rev. B **39**, 2084 (1989).

[23] J. Tobochnik and G. V. Chester, Phys. Rev. B **20**, 3761 (1979); J. E. Van Himbergen and S. Chakravarty, *ibid.* **23**, 359 (1981).

[24] K. J. Strandburg, Rev. Mod. Phys. **60**, 161 (1988).

[25] D. C. Glattli, E. Y. Andrei, and F. I. Williams, Phys. Rev. Lett. **60**, 420 (1988); D. S. Greywall and P. A. Busch, *ibid.* **67**, 3535 (1991).

[26] R. Geer, T. Stoebe, T. Pitchford, and C. C. Huang, Rev. Sci. Instrum. **62**, 415 (1991).

[27] R. Geer, C. C. Huang, R. Pindak, and J. W. Goodby, Phys. Rev. Lett. **63**, 540 (1989).

[28] C. Rosenblatt and N. Amer, Appl. Phys. Lett. **36**, 432 (1980).

[29] E. B. Sirota, P. S. Pershan, L. B. Sorenson, and J. Collet, Phys. Rev. B **36**, 2890 (1987).

[30] J. D. Bologa and C. W. Garland, Rev. Sci. Instrum. **48**, 105 (1977).

[31] T. Pitchford, G. Nounesis, S. Dumrongrattana, J. M. Viner, C. C. Huang, and J. W. Goodby, Phys. Rev. A **32**, 2422 (1986).

[32] In principle, we would like to determine the measured heat capacity of thick films in an appropriate unit and make a direct comparison with the data from the bulk calorimeter. However, no appropriate method allows us to determine the film thickness of thick films (greater than

a few hundred layers) with desired accuracy (better than 10%).
[33] J. T. Ho (private communication).
[34] R. Geer, T. Stoebe, C. C. Huang, R. Pindak, J. W. Goodby, M. Cheng, J. T. Ho, and S. W. Hui, Nature **355**, 152 (1992).
[35] R. Bruinsma and G. Aeppli, Phys. Rev. Lett. **48**, 1625 (1982).
[36] A. M. Levelut, J. Phys. (Paris) Colloq. **37**, C3-51 (1976).
[37] M. Chen, J. T. Ho, S. W. Hui, and R. Pindak, Phys. Rev. Lett. **61**, 550 (1988).

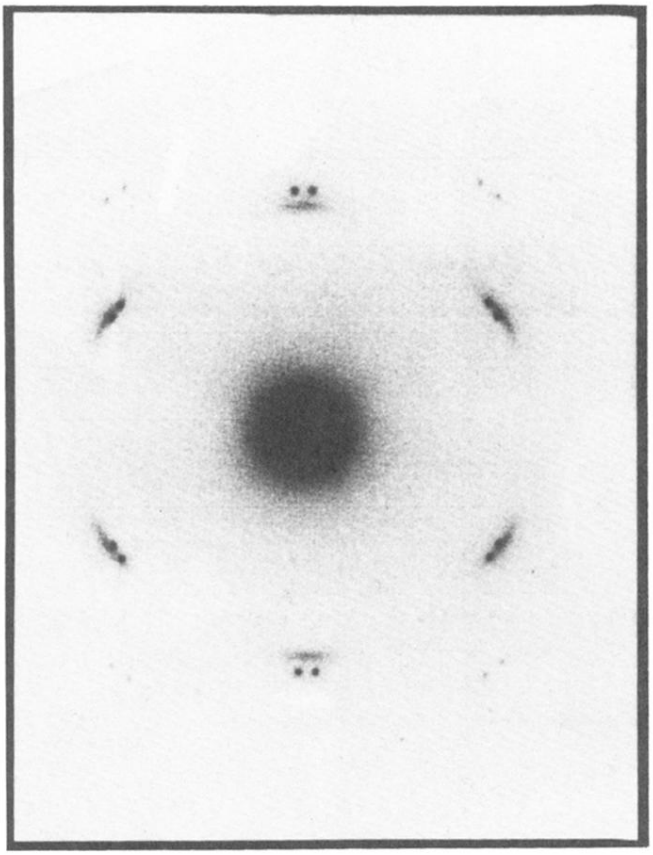

FIG. 9. Electron-diffraction pattern from a five-layer 75OBC film. The sixfold symmetric diffuse scattering identifies interior hexatic order, while two sets of Cry-*E* spots reflect separate Cry-*E* surface domains.